

University of Mississippi

eGrove

Electronic Theses and Dissertations

Graduate School

2013

Mechanical Properties Of Portland Cement And Its Constituents At The Nano-Level

Brent French

University of Mississippi

Follow this and additional works at: <https://egrove.olemiss.edu/etd>



Part of the [Civil Engineering Commons](#)

Recommended Citation

French, Brent, "Mechanical Properties Of Portland Cement And Its Constituents At The Nano-Level" (2013). *Electronic Theses and Dissertations*. 534.

<https://egrove.olemiss.edu/etd/534>

This Thesis is brought to you for free and open access by the Graduate School at eGrove. It has been accepted for inclusion in Electronic Theses and Dissertations by an authorized administrator of eGrove. For more information, please contact egrove@olemiss.edu.

MECHANICAL PROPERTIES OF PORTLAND CEMENT AND ITS CONSTITUENTS AT THE NANO-LEVEL

A Thesis

presented in partial fulfillment of requirements

for the degree of Master of Science

in the Department of Civil Engineering

The University of Mississippi

by

Brent Alexander French

May 2013

Copyright Brent A. French

ALL RIGHTS RESERVED

ABSTRACT

The following is a summary of research for a portion of the project titled *Nano to Continuum Multi-Scale Modeling Techniques and Analysis For Cementitious Materials Under Dynamic Loading* in association with North Carolina Agricultural & Technical State University and the US Army. This research investigates several attempts at creating a better Portland cement model at the atomistic level through molecular dynamics simulations. These models are modified to simulate damage to the basic cement structure, and are simulated using several combinations of forcefields and molecular dynamics tools.

Experimental techniques such as nanoindentation, atomic force microscopy, and x-ray diffraction are applied to Portland cement samples to correlate mechanical properties among these techniques, as well as the numerical simulations.

LIST OF ABBREVIATIONS

A – cross-sectional area of the indentation

AFM – atomic force microscopy

C₃S – tricalcium silicate

Ca - calcium

CH – calcium hydroxide

COMPASS – Condensed-phase Optimized for Atomic Simulation Studies

C-S-H – calcium silicate hydrate

E – Young's modulus

E_i – Young's modulus of the indenter

E_r – reduced modulus

ERDC – Engineer Research and Development Center

GULP – General Utility Lattice Program

H – hardness

HD C-S-H – high density calcium silicate hydrate

LD C-S-H – low density calcium silicate hydrate

MD – molecular dynamics

mN – milliNewton

NCPA – National Center for Physical Acoustics

NI – nanoindentation

NIRG – Nano Infrastructure Research Group

NIRL – Nano Infrastructure Research Laboratory

nm – nanometer

P – force applied

RVE – representative volume element

Si -silicon

XRD – X-ray diffraction

ν – Poisson's ratio

ν_i – Poisson's ratio of indenter

TABLE OF CONTENTS

ABSTRACT	ii
LIST OF ABBREVIATIONS.....	iii
TABLE OF CONTENTS.....	v
LIST OF TABLES.....	viii
LIST OF FIGURES.....	ix
1. INTRODUCTION.....	1
1.1. Background.....	1
1.1.1. Clinker Phases.....	1
1.1.2. Hydration.....	2
1.1.3.....	3
Manufacturing.....	3
1.1.4. X-Ray Diffraction.....	4
1.1.5. Atomic force microscopy.....	4
1.1.6. Nanoindentation.....	5
1.2. Motivation.....	9
1.3. Objectives.....	11

1.4.	Approach	11
2.	MOLECULAR DYNAMICS.....	14
2.1.	Molecular dynamics literature review	14
2.1.1.	Thermodynamic ensemble	15
2.1.2.	Effect of varying forcefields.....	19
2.1.3.	Effect of varying MD tools.....	20
2.2.	Input parameters	23
2.3.	Effect of varying MD tools and forcefields.....	24
2.4.	Effect of varying cell sizes.....	25
2.5.	Effect of varying chain lengths	28
3.	Experimental.....	33
3.1.	Nano cement manufacturing	33
3.2.	XRD.....	35
3.3.	Sample preparation	38
3.3.1.	ERDC Sample preparation procedure	42
3.3.2.	ERDC Grinding/polishing procedure.....	43
3.4.	Atomic Force Microscopy.....	43
3.4.2.	Phase analysis.....	47
3.5.	Nanoindentation.....	52

4. CONCLUSION	71
4.1. Future work	73
BIBLIOGRAPHY	61

LIST OF TABLES

Table 1: Portland cement clinker information	2
Table 2: C ₃ S Components	33
Table 3: Effect of varying the maximum applied load in nanoindentation tests	55
Table 4: Lattice parameters and information of MD structures	80
Table 5: Calcium hydroxide cell parameters	81

LIST OF FIGURES

Figure 1: Low density C-S-H and high density C-S-H globules	3
Figure 2: C ₃ S unit cell.....	3
Figure 3: C ₃ S 2x2x2 Supercell.....	3
Figure 4: A. C ₃ S with w/c ratio 0.60, B. C ₃ S with w/c ratio 0.80	34
Figure 5: A. C ₃ S with w/c ratio 1.00, B. C ₃ S with w/c ratio 1.20, C. C ₃ S with w/c ratio 1.40	35
Figure 6: Nanoindenter and Microscope	6
Figure 7: Berkovich tip.....	6
Figure 8: Principle of Indentation Test.....	7
Figure 9: Nanoindentation hysteresis curve	8
Figure 10: Load vs. time plot of nanoindentation test	9
Figure 11: The expanding growth of worldwide cement consumption	10
Figure 12: Nano Characterization Breakdown	12
Figure 13: Effect of varying MD tools & forcefields with C-S-H model.....	25
Figure 14: Tobermorite 11Å Chain with Ca/Si ratio 1.00	29

Figure 15: Tobermorite 11Å Chain with Ca/Si ratio 0.83	30
Figure 16: Tobermorite 11Å Chain with Ca/Si ratio 0.66	31
Figure 17: MD simulation on the effect of chain length	31
Figure 18: Bruker D8 Powder X-Ray Diffractometer at NCPA	36
Figure 19: Top: C ₃ S XRD Spectrum from literature; Bottom: C ₃ S XRD spectrum from experiment	37
Figure 20: Top: HCP XRD Spectrum from literature; Bottom: HCP XRD spectrum from experiment	37
Figure 21: Buehler Grinding/Polishing Table	38
Figure 22: AFM image of a poorly polished cement sample	39
Figure 23: Unobstructed vs. obstructed nanoindenter tip paths	39
Figure 24: Nanoindentation test of a poorly polished Portland cement specimen at a max applied load of 1.5 mN	40
Figure 25: Nanoindentation test of a poorly polished Portland cement specimen at a max applied load of 1 mN	41
Figure 26: AFM of hardened Portland cement paste with phase ID	45
Figure 27: Portland cement topographic image and 3D image from MountainMaps	46
Figure 28: Phase contrast image and histogram of Portland cement (5 micron scan size)	48

Figure 29: Phase contrast image and histogram of Portland cement (500 nm scan size).....	49
Figure 30: Phase contrast image and histogram of Portland cement (500 nm scan size).....	50
Figure 31: 10x10 Nanoindentation mapping.....	53
Figure 32: Effect of varying the maximum applied load in nanoindentation tests on Portland cement.....	54
Figure 33: Hardened Portland cement paste specimen ready for nanoindentation	56
Figure 34: Nanoindentation of cement phase distribution histogram	57
Figure 35: Frequency distribution of elastic moduli of Portland cement nanoindentation	58
Figure 36: Hysteresis curves of C-S-H (from 15-35 GPa).....	59
Figure 37: Hysteresis curves of CH (from 35-60 GPa).....	60
Figure 38: Hysteresis curves of other materials in Portland cement (0-15 GPa and 60-max GPa)	60
Figure 39: Nanoindentation results of hydrated C ₃ S and cement.....	61
Figure 40: C ₃ S (w/c: 1.20) after preparation at ERDC	62
Figure 41: MD structures lattice parameter key	80
Figure 42: Calcium hydroxide unit cell	81
Figure 43: Calcium Hydroxide 2x2x2 Supercell.....	81

Figure 44: C-S-H unit cell from MIT	81
Figure 45: C-S-H Structure from MIT, 2x2x2 Supercell	83
Figure 46: C ₃ S Unit Cell	84
Figure 47: C ₃ S 2x2x2 Supercell	86
Figure 48: Frequency of elastic moduli of Portland cement with 1 mN max applied load	87
Figure 49: Frequency of elastic moduli of Portland cement with 1.5 mN max applied load	87
Figure 50: Frequency of elastic moduli of Portland cement with 10 mN max applied load	87
Figure 51: Frequency of elastic moduli of Portland cement with 50 mN max applied load	87
Figure 52: Frequency of elastic moduli of C ₃ S with 5 mN max applied load	87
Figure 53: Frequency of elastic moduli of C ₃ S with 30% Portland cement with 5 mN max applied load.....	87
Figure 54: Frequency of elastic moduli of C ₃ S with 30% Portland cement and gypsum with 5 mN max applied load.....	87
Figure 55: Frequency of elastic moduli of C ₃ S with 5 mN max applied load after ERDC preparation	87
Figure 56: Phase distribution of hardened Portland cement paste (1 micron scan size).....	87
Figure 57: Topographic AFM image of hardened Portland cement paste (5 micron scan size) ...	87

Figure 58: AFM image of cement from Nanovea AFM (10 micron scan size)87

1. INTRODUCTION

1.1. Background

The most widely used manufactured material in the world is Portland cement concrete with 2,297 million tons consumed in 2005 and a 2.5% annual growth [Rubenstein, 2012], yet it is still an extremely complex material. Because of this, it is important to study all components involved in the manufacturing of Portland cement from atomic level and up. Studying calcium silicate hydrate (C-S-H) is very important in the determination of the physical properties of the Portland cement paste because it is the main hydration product that makes up approximately two-thirds of the volume of solids in hydrated cement paste (it is hyphenated because it is not a well-defined compound) [Allen et al. 2007]. The second hydration product is calcium hydroxide (CH).

1.1.1. Clinker Phases

Cement is composed mainly of four unhydrated clinker phases (see Table 1). Tricalcium silicate (C_3S) is the most prominent component, making up approximately 50%. The presence of oxides results in small impurities in commercially available cement. The “impure” C_3S is known by the mineral name “alite.” Dicalcium silicate (C_2S) makes up approximately 25% of the cement paste, and this impure C_2S is known by the mineral name “belite.” Tricalcium aluminate (C_3A) makes up approximately 12% of the cement paste. Tetracalcium aluminoferrite makes up

approximately 7% of the cement paste. These amounts vary among commercially available cements and usually have residual minor compounds [Neville et al. 1973].

Mineral Name	Component	Formula	Composition	Reactivity	Properties
Alite	C ₃ S	3CaO SiO ₂	50 %	Hydrates & hardens quickly	Early strength & initial setting
Belite	C ₂ S	2CaO SiO ₂	25 %	Hydrates & hardens slowly	Later strength
Aluminate	C ₃ A	3CaO Al ₂ O ₃	15 %	Reacts with water creating heat	Favored sulfate resistance
Ferrite	C ₄ AF	4CaO Al ₂ O ₃ Fe ₂ O ₃	10 %	Reacts less with water than aluminate	Reduces clinkering temp.
Total	C-S-H		100 %		

Table 1: Portland cement clinker information

1.1.2. Hydration

Hydration of cement is what happens when chemical reactions take place in different stages as a specific amount of water is added to the unhydrated cement powder. The tricalcium silicate hydrates the fastest out of the four main clinker phases, producing the C-S-H gel and CH.

Dicalcium silicate hydrates more slowly than tricalcium silicate, continuing the production of C-S-H gel and CH for the latter portion of the hydration process [Selvam et al. 2009].

In a study by Tennis and Jennings [2000], two types of C-S-H are identified with different densities: a high density C-S-H portion (HD C-S-H) and a low density portion (LD C-S-H) which have a 24% gel porosity and a 37% gel porosity, respectively. These two separate cement types are composed of “globules” with a 5.6 nm diameter (see Figure 1). Though the nanoporosity and gel porosity of C-S-H are intrinsic, the proportion of LD C-S-H and HD C-S-H varies by

volume depending on the w/c ratio [Al-Ostaz et al. 2010]. In this research, LD C-S-H and HD C-S-H are identified through AFM and nanoindentation.

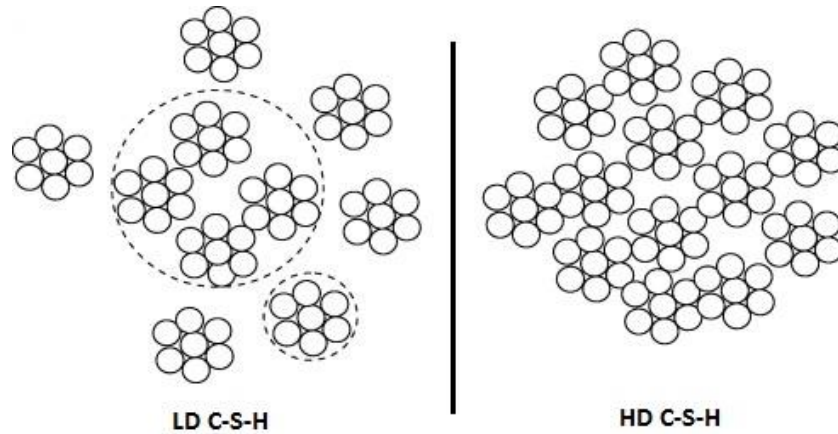


Figure 1: Low density C-S-H and high density C-S-H globules

1.1.3. Manufacturing

Industrial cement manufacturing

Type I/II Portland cement is commercially manufactured using primarily the raw calcium silicate materials: lime (approximately 60%-67%), silica (approximately 17%-25%), alumina (approximately 2%-8%), and iron oxide (approximately 0%-6%). The lime is obtained from mining limestone, shells, or chalk, the silica is obtained from sand or fly ash, the alumina is obtained from clay, shale, or fly ash, and the source of the iron oxide is iron ore. Once these materials are mined or quarried, they are transported to manufacturing facility where they are crushed and milled into a powder. The powder is then transferred to kilns where it is preheated and then fully heated to approximately 1400°C until the clinkers are created. The cement clinkers are then transferred to a cooling area that can send the excess heat back to the

preheater. The clinkers are then ground once more to create the final Portland cement product [Huntzinger and Eatmon, 2009].

1.1.4. X-Ray Diffraction

X-Ray diffraction (XRD) is a non-destructive analytical technique which can be used to identify and confirm a crystalline structure, phase, and other properties of a specimen. It is defined as an X-Ray scattering method that is based on measuring the intensity of the X-Ray beam that is shot through the specimen. Powder XRD is the specific technique used in this research to verify the phase and crystallinity of the C_3S created in the nano-cement manufacturing process. The results are in the form of output spectrum which is compared to defined spectrum associated with the specimen on an online mineralogy database.

1.1.5. Atomic force microscopy

Atomic force microscopy (AFM) is a form of scanning probe microscopy that has an extremely high resolution which provides images on even the atomistic/molecular level. The resolution is so high that it is far beyond the optical diffraction limit, so, AFM uses a microscopic cantilever to “feel” the surface of a sample and, in turn, generate an image of it. However, the nano-tips on the end of the cantilevers do not actually touch the surface of the sample, but van der Waals forces are present which causes the tip come within just 10\AA of physical contact with the surface. AFM is useful in studying cement samples because the two forms of C-S-H can be identified (high-density C-S-H and low-density C-S-H).

There are two modes commonly used in AFM: tapping mode and contact mode. In tapping mode, the nano-tip “taps” the surface of the sample by oscillating up and down as it scans back

and forth across the surface. The images produced by tapping mode tend to be clearer than images produced in contact mode, and it can scan an image over a larger area. However, the surface of the sample must be much smoother for tapping mode and the imaging process is much longer than contact mode. In contact mode, the nano-tip simply moves back and forth across the surface of the sample without oscillating up and down. The primary advantages to contact mode are that it has the ability to scan surfaces that have not been thoroughly and properly prepared, and contact mode scans are performed much faster than tapping mode scans.

An image is generated via laser reflection off of the top of the nano-tip which is received through a photodiode. As the cantilever deflects as it moves across the surface, the reflection of the laser moves, allowing the computer software (NanoScope 6.6) to generate an image in a raster pattern in real-time. This image can be further processed and studied with post-hoc analysis software (MountainsMap 6.2) which aids in phase analysis for Portland cement.

Two types of AFM images are utilized in this research: topographic images and phase contrast images. Topographic images are produced as a direct output of the up and down motion of the cantilever moving across the surface of the specimen. Phase images measure energy dissipation between the cantilever tip and the surface of the specimen. It is best used for the characterization of components of heterogeneous materials.

1.1.6. Nanoindentation

The mechanical properties of Type I/II Portland cement and C_3S , such as elastic modulus and hardness, are obtained through many nanoindentation tests using various loads over multiple

indent locations. The nanoindenter used is the NANOVEA M1 Hardness Tester with a Berkovich tip (three-sided pyramid, Figure 3).



Figure 2: Nanoindenter and Microscope

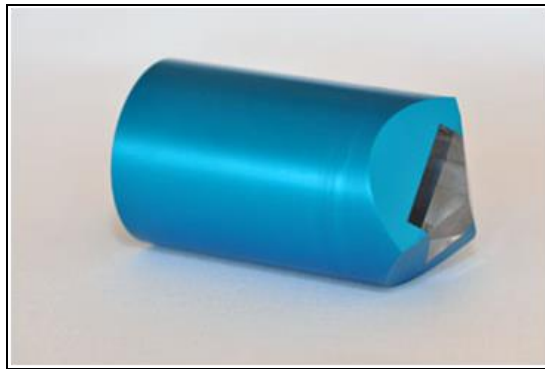


Figure 3: Berkovich tip

It is beneficial to physically analyze the mechanical properties of cement at multiple scales. At the nanoscale, nanoindentation is currently the best solution for determining local mechanical properties quantitatively. AFM force deflection techniques are non-destructive to the

specimen, but nanoindentation actually penetrates into the specimen, leaving a permanent indentation. This consists of two phases: loading phase and unloading phase. A small tip (with an area on the nanometer to micrometer scale), usually made of diamond, is forced down onto the specimen. Equation 1 is used to measure the hardness, H , by dividing the force applied, P , by the projected contact area, A :

$$H = \frac{P}{A}$$

Equation 1

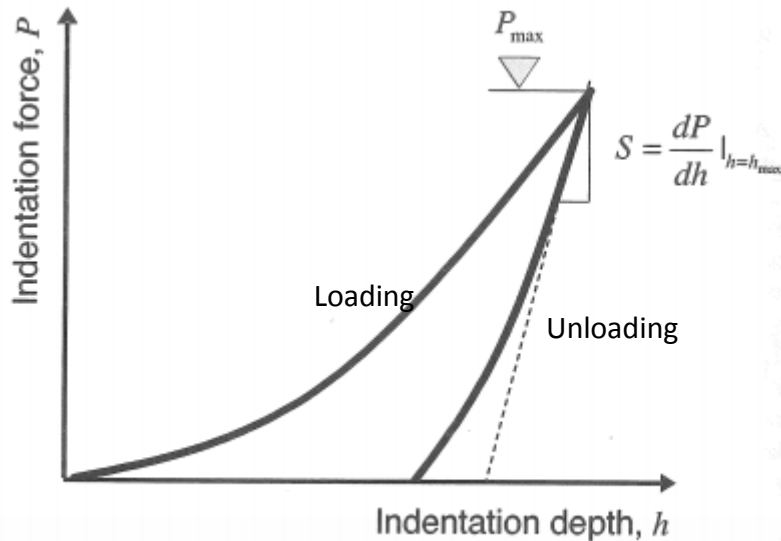


Figure 4: Principle of Indentation Test

The reduced modulus is determined using Equation 2:

$$E_r = \frac{\sqrt{\pi}}{2} \frac{S}{\sqrt{A_c}} = \frac{\sqrt{\pi}}{2} \frac{1}{C} \frac{1}{\sqrt{A_c}}$$

Equation 2

where S is the contact stiffness, C is the compliance (inverse of contact stiffness), and A_c is the projected contact area. E_r can be used to find Young's modulus of the specimen using Equation 3:

$$\frac{1}{E_r} = \frac{1 - \nu^2}{E} + \frac{1 - \nu_i^2}{E_i}$$

Equation 3

where E is Young's modulus, ν is Poisson's ratio, E_i is Young's modulus of the indenter, and ν_i is Poisson's ratio of the indenter [Tchon, 2010].

The load of an indentation varies as a function of the depth of the indentation into a specimen, and it is continuously monitored and measured throughout the process. [Dormieux, 2005] Figure 5 represents a typical hysteresis curve (load vs. indentation depth) of a nanoindentation test performed at NIRG laboratory.

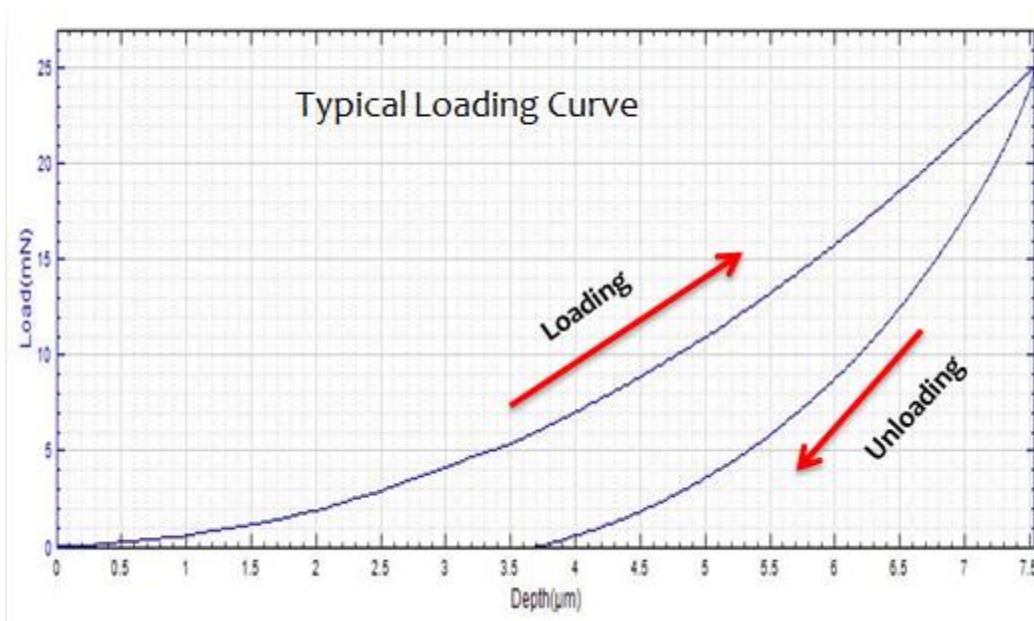


Figure 5: Nanoindentation hysteresis curve

Figure 6 represents a typical loading vs. time plot. The flat portion of the beginning of the plot represents the amount of time it takes the indenter tip to reach the surface of the specimen. Once contact has been made, the plot begins to make a linear approach to the previously specified maximum applied load, with a slope equal to approach speed. Once the peak has been reached, the plot begins to decrease linearly at a slope equal to the negative of the approach speed.

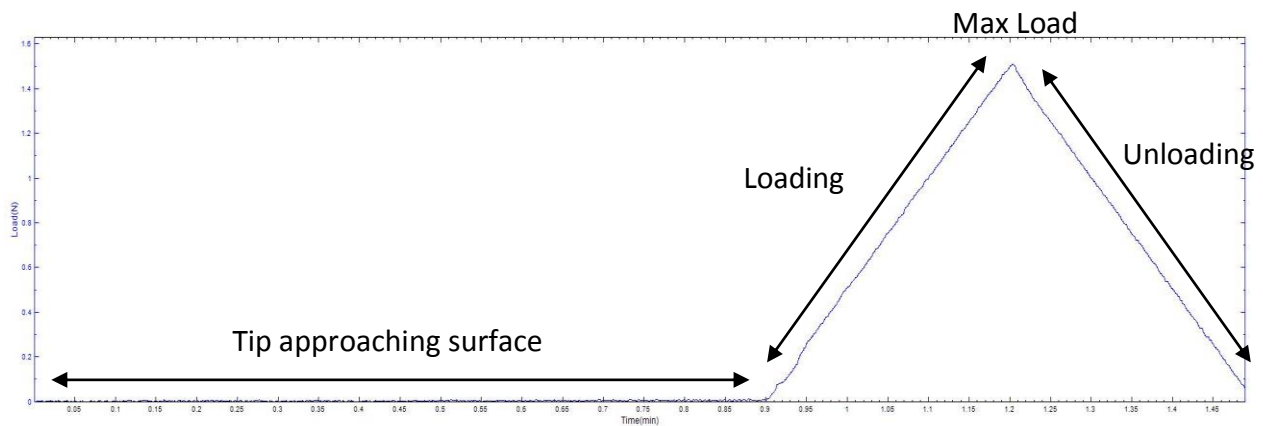


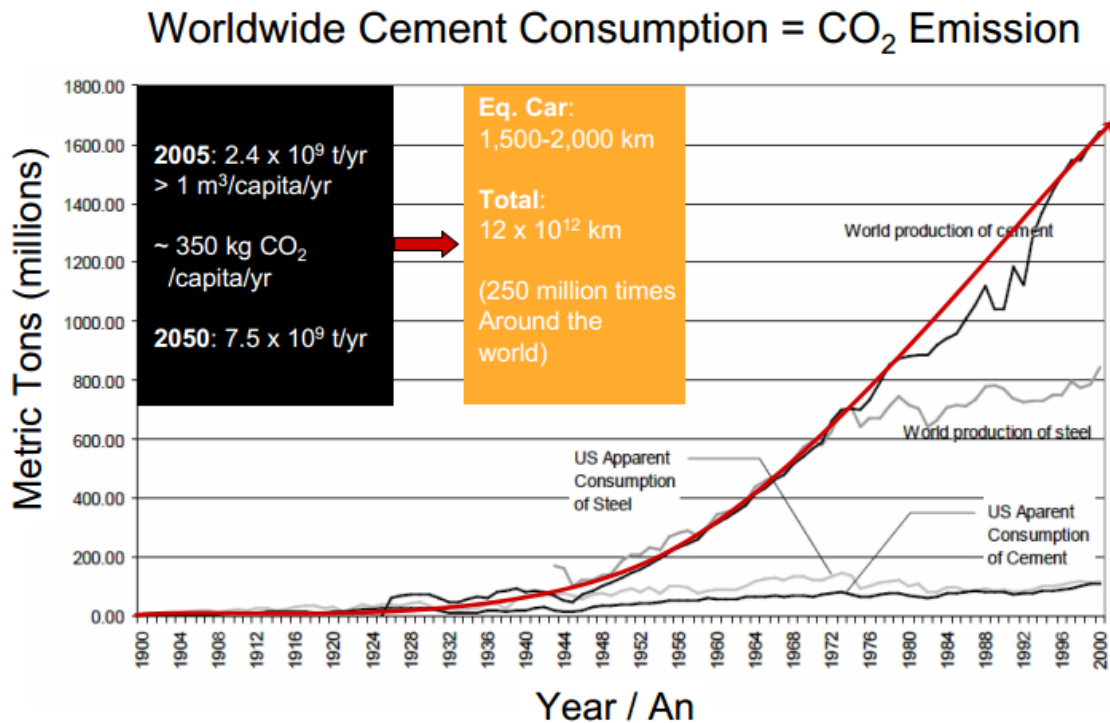
Figure 6: Load vs. time plot of nanoindentation test

1.2. Motivation

The two main issues facing the current cement manufacturing industry are the large amount carbon dioxide emissions and the high rate of energy consumption.

Due to the vast amount of cement being produced globally (see Figure 7), it is a large contributor to the earth's total carbon dioxide (CO₂) emissions at 5% and also approximately 18% of the total greenhouse gas emissions. The majority of the world's cement production comes from China, India, and the United States. The world relies strongly on cement and consumption of it grows 2.5% every year. Current cement manufacturing techniques involve

heating materials such as limestone to extreme temperatures as high as 1450° C where calcination occurs. Constant production at these high temperatures requires a great amount of energy, which leads to many emissions. The production of one ton of cement requires 60-130 kg of fuel and 110 kWh of electricity. This amount of energy consumption results in approximately 900 kgCO₂/t of emissions. These numbers vary slightly worldwide due to the use of different types of fuel sources, but on average, the three highest cement-producing countries create 900-935 kgCO₂/t. [Rubenstein, 2012]. Studying cement at the nano-level and alternative methods to producing cement can present a solution to the current emission problem facing the cement industry.



Chaturvedi, S. and Ochsendorf, J., "Global Environmental Impacts Due to Concrete and Steel," *Structural Engineering International*, 14/3, Zurich, Intl. Assoc. of Bridge and Structural Engineers, August 2004, 198-200.

Franz-Josef Ulm – What's the matter with concrete? – September 2007

Figure 7: The expanding growth of worldwide cement consumption

1.3. Objectives

The main objectives of this research are:

- Assess mechanical properties of C-S-H and its constituents theoretically using molecular dynamics simulations
- Correlate the detailed nano-structure of Portland cement using atomic force microscopy
- Manufacture pure C_3S alone from its chemical composition
- Assess the mechanical properties of C-S-H and its constituents, produced by a reaction of C_3S and water, through nanoindentation

1.4. Approach

To achieve the objectives stated in Section 1.3, a thorough numerical and experimental study C-S-H and its constituents must be applied. Figure 8 shows the breakdown of the nano-characterization of Portland cement and its constituents for this study. Several MD tools will be used to study the effect of various forcefields on the molecular structures of the cementitious materials. These MD tools and forcefields will also be used to analyze the effect of changing the RVE size of the molecular structures. The effect of varying the chain length of calcium-silicate chains will also be studied.

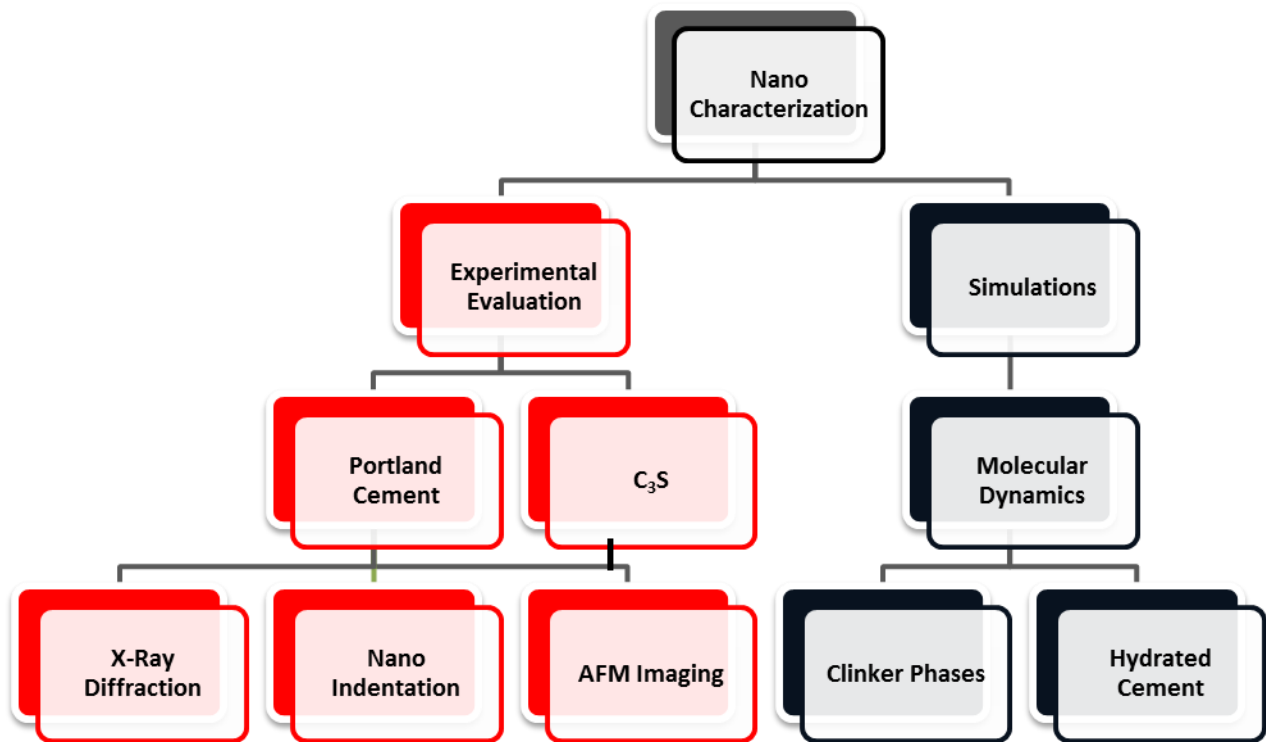


Figure 8: Nano Characterization Breakdown

Atomic force microscopy is a trusted tool that can be beneficial to studying composition of cementitious materials at the nano-scale. Portland cement specimens will be prepared and polished for phase analysis. Low-density and high-density C-S-H globules can be distinguished as AFM scan sizes reach 5 microns and smaller. This phase analysis will be performed on samples that have been polished thoroughly and samples that have been insufficiently polished to prove the necessity of proper sample preparation

The constituents of hardened Portland cement paste must be manufactured through a process utilizing the chemicals of which they are composed. The main hydrating product and the most abundant of the C-S-H constituents, C_3S , will be manufactured and then validated through XRD.

The physical mechanical properties of the cementitious materials will be obtained through numerous nanoindentation tests. Through these tests, the effects of applying various sample preparation techniques will be studied. The maximum applied load of the nanoindentation tests will be varied throughout the testing to examine the effect of loading. Histograms containing the frequencies of the occurrence of the mechanical properties of the Portland cement samples will be studied to verify the presence of LD C-S-H and HD C-S-H.

2. MOLECULAR DYNAMICS

The numerical portion of this research includes the study of C-S-H and its constituents at the molecular level using the molecular dynamics software Accelrys Materials Studio. The effect of various forcefields, MD tools, cell sizes, and chain lengths are studied in this section.

2.1. Molecular dynamics literature review

In general, there are two atomistic simulation techniques that are widely used: lattice dynamics and molecular dynamics. Lattice dynamics solves Newton's equation of motion with an analytical approach and then a statistical mechanical treatment [Born et al., 1954]. On the other hand, molecular dynamics solves Newton's equation of motion with a numerical approach. Unlike lattice dynamics, positions and velocities of atoms are not bound to solids, and particles are involved in time-dependent motion. Though it requires more computational time, molecular dynamics provides more accurate results than lattice dynamics [Parker et al., 2001].

Molecular dynamics utilizes microscopic simulations and atomic positions and velocities to obtain macroscopic properties. Energy minimization is a procedure that brings the total energy of a system to its minimum by adjusting the positions of atoms and cell parameters. Then, a stable conformation is produced after the structure is created and refined. Thermodynamic variables, such as temperature and pressure control, are used in the dynamics simulations. The

kinetic energy generated from temperature control help the molecules move over multiple potential barriers. A global minimum is obtained through anneal dynamics. In a study by Wu et al., this process is performed with the temperature periodically increasing from room temperature to 500 K and back again. The energy minimized structure is then used as the initial structure for the dynamics simulation. The Maxwell-Boltzmann distribution gives the initial velocity for each atom. Each atom is scaled to heat the system to the target temperature. The forces, velocities, and positions of each atom are then found based on potential from solving Newton's equation of motion. Bringing the system to equilibrium usually requires many iterations and a large CPU run time. Thermodynamic equilibrium is reached when energy and temperature vs. time fluctuate around their averages until they become constant. Finally, after the dynamic simulation has been completed, elastic constants are determined from the deformed structure [Wu et al., 2011].

2.1.1. Thermodynamic ensemble

The thermodynamic state of a system is defined by variable parameters such as number of atoms, temperature, volume, and pressure. The canonical thermodynamic ensemble, which is used in this research, maintains a constant number of atoms (N), volume (V), and temperature (T). It is commonly referred to as NVT [Alkhateb et al., 2008].

Forcefields

Force fields are used in molecular dynamics simulations to calculate potential energies in the system with respect to nuclear positions and model the interactions among atoms. For bonded terms, the total energy calculated includes the summation of energies from bond stretching,

bond rotation, bond torsion, and inversion. For non-bonded terms, the energies are calculated from van der Waals and electrostatic forces. The nuclei have relatively large masses for these systems, so Newton's equation of motion can be used in the form:

$$- d E_m/dR=m d R^2/dt^2$$

Equation 6

for basic force field calculations where E_m is the force field, R is the location of the nucleus in space, m is the mass of the nucleus, and t is time. Force fields were originally created very generically so they could be used in many various applications. Later, force fields such as COMPASS (Condensed-phase Optimized Molecular Potentials for Atomistic Simulation Studies) were created to provide more powerful and accurate results for a broad range of molecular dynamics simulations.

2.1.1.1. COMPASS

COMPASS is a strong forcefield used primarily for condensed-phase materials. It is an ab initio force field, which means it uses computational methods to simulate atomistic interactions using quantum mechanics principles on the Angstrom-nanoscale and femto-picosecond time scale.

This is useful because most of the input parameters for the system are derived from ab initio data. COMPASS uses condensed-phase properties, ab initio data and empirical data for molecules in isolation for parameterization and validation. It can predict very accurately the structural, conformational, vibrational, and thermophysical properties of a molecular system simultaneously. However, unlike previous forcefields, it can do all of this for many various molecules in both isolated and condensed phases in various temperature and pressure conditions which produces results very similar to experimental data [Accelrys, 2012].

The functional form of COMPASS is represented in :

$$\begin{aligned}
E_{total} = & \sum_b [K_2(b - b_0)^2 + K_3(b - b_0)^2 + K_4(b - b_0)^2] \\
& + \sum_\theta [K_2(\theta - \theta_0)^2 + K_3(\theta - \theta_0)^2 + K_4(\theta - \theta_0)^2] \\
& + \sum_\phi [K_{1\phi}(1 - \cos \phi) + K_{2\phi}(1 - \cos 2\phi) + K_{3\phi}(1 - \cos 3\phi)] \\
& + \sum_\chi K_{2\chi}(\chi - \chi_0)^2 + \sum_{b,\theta} K_{b\theta}(b - b_0)(\theta - \theta_0) + \sum_{b,\theta} (b - b_0)[K_{1b} \cos \phi \\
& + K_{2b} \cos 2\phi + K_{3b} \cos 3\phi] \\
& + \sum_{b,\theta} (\theta - \theta_0)[K_{1\theta\phi} \cos \phi + K_{2\theta\phi} \cos 2\phi + K_{3\theta\phi} \cos 3\phi] \\
& + \sum_{\theta,\phi} (\theta' - \theta'_0)(\theta - \theta_0) + \sum_{\theta,\phi} K_{\theta,\phi}(\theta' - \theta'_0)(\theta - \theta_0) \cos \phi + \sum_{ij} \frac{q_i q_j e}{r_{ij}} \\
& + \sum_{ij} \varepsilon_{ij} \left[2 \left(\frac{r_{ij}^0}{r_{ij}} \right)^9 - 3 \left(\frac{r_{ij}^0}{r_{ij}} \right)^6 \right]
\end{aligned}$$

Equation 7

where terms one through ten represent the valence terms signify internal coordinates of angle θ , bond b , out-of-plane angle χ , and torsion angle ϕ . Terms five through eight represent cross-coupling terms include combinations of two or three internal coordinates which are important in predicting vibration frequencies and structural variations from conformational changes. For non-bond interactions, represented by the last two terms, a Lennard-Jones 9-6 function is used for the van der Waals term and a Coulombic function is used for an electrostatic interaction.

Scientists are currently attempting to broaden the possible applications of the COMPASS force field to more and more molecular systems and, in time, most common organic and inorganic materials being researched today. As of now, most common organic, inorganic small molecules, polymers, small gas molecules, some metal ions, metal halides, metal oxides, metals, and zeolites meet the requirements of COMPASS [Sun, 1998].

2.1.1.2. Dreiding

The Dreiding forcefield uses explicit parameters which are derived by a rule-based approach. It is a purely diagonal forcefield that has harmonic valence terms and a cosine-Fourier expansion torsion term. The Lennard-Jones potential is used to define the van der Waals interactions and atomic monopoles and a distance-dependent Coulombic term is used to define electrostatic interactions. A Lennard-Jones 12-10 potential is used to define the hydrogen bonding. The Dreiding forcefield's best applications are for biological, organic, and main-group inorganic molecules. It can also be used for geometries, conformational energies, intermolecular binding energies, and crystal packing [Mayo et al., 1990].

expresses the potential energy of the Dreiding forcefield:

$$\begin{aligned}
E_{total}^{Dreiding} &= E_{val} + E_{nb} = (E_B + E_A + E_T + E_l) + (E_{vdw} + E_Q + E_{hb}) \\
&= \frac{1}{2}k_s(R - R_s)^2 + \frac{1}{2}C_{IJK}[\cos\theta_{IJK} - \cos\theta_J^0]^2 + \frac{1}{2}V_{JK}\{1 - \cos[n_{JK}(\varphi - \varphi_{JK}^0)]\} \\
&+ \frac{1}{2}K_{inv}(\psi - \psi_0)^2 + D_0[\rho^{-12} - 2\rho^{-6}] + 332.0637\left(\frac{Q_i Q_j}{\epsilon R_{ij}}\right) \\
&+ D_{hb}\left[5\left(\frac{R_{hb}}{R_{DA}}\right)^{12} - 6\left(\frac{R_{hb}}{R_{DA}}\right)^{10}\right]\cos(\theta_{DHA})
\end{aligned}$$

Equation 8

where E_b , E_A , E_T , E_l , and E_{hb} are the energies of bond stretch, bond angle bend, dihedral angle torsion, inversion, and hydrogen bond, respectively; K , C , and V are constants; D_0 is van der Waals well depth; $\rho = R/R_0$ is the scaled distance; R_0 is van der Waals bond length; Q is the charge; D_{hb} , R_{hb} , and R_{DA} are hydrogen parameters.

2.1.2. Effect of varying forcefields

Various forcefields and MD tools are attempted to determine which combination will provide the results most similar to those in the literature and experimental testing of the physical specimens. For example, the application of the COMPASS forcefield on a C-S-H model using the Forcite MD tool will not produce the same results as the application of the Dreiding forcefield on the same model using the same MD tool.

MD Tools

2.1.2.1. GULP

GULP, Discover, and Forcite Plus are the three molecular dynamics tools used in this study. The General Utility Lattice Program (GULP) is a software tool that originally created as input file-

driven program for interatomic potential fitting. It is now capable of performing energy minimizations, phonon calculations, and more. The use of symmetry for solids to accelerate calculations is what sets GULP apart from similar MD tools [Accelrys, 2006].

2.1.2.2. Discover

Another MD tool is Discover. It is capable of operating with molecular systems that contain a broad range of material types. The structural characterization and properties of molecules, materials, and biological compounds can also be found using Discover. The structures, energies, and properties of many systems can be easily calculated through dynamics simulations, energy minimizations, and conformational searches using Discover's many different available forcefields [Accelrys, 2006].

2.1.2.3. Forcite Plus

Forcite Plus is a third MD tool that is used because the COMPASS and Dreiding forcefields are available in it. It is a unique tool because a classical forcefield represents the potential energy surface, where atomic nuclei move. With Forcite Plus, it is possible to perform energy calculations, geometric optimizations, dynamic simulations, and mechanical properties calculations [Accelrys, 2006].

2.1.3. Effect of varying MD tools

The forcefields that are currently compatible with C-S-H structures are not available on all MD tools. The COMPASS forcefield is compatible with the Discover and Forcite Plus MD tools but not GULP. Similarly, the Dreiding forcefield is incorporated in the Forcite Plus and GULP MD tools but not Discover.

2.1.4. Effect of varying cell sizes

The crystalline structures used in this paper are obtained as unit cells. These unit cells are the smallest possible definition of the crystal, and it is sometimes unstable to run a molecular dynamics simulation on just the unit cell alone. However, this single unit cell can be replicated on any face of the lattice to create a larger unit (supercell) that will yield more stable results, consequently at a longer calculation time. No objects are destroyed in this process, but the relationships between objects are redefined. Therefore, translationally symmetric atoms are unrelated symmetrically and are free to move independently.

Some molecular models of C-S-H and its components contain a small amount of atoms and may produce inaccurate results from molecular dynamics simulations using certain MD tools. It is possible to simulate an increase in the scale of a molecular model symmetrically by creating a supercell which simply replicates the model a specific number of times in the X, Y, or Z directions. After a molecular structure has been through an energy minimization and had a thermodynamic ensemble applied to it, the elastic properties are not always isotropic in the X, Y, and Z directions. In cases like this, a supercell can be expanded on certain axes but not necessarily all of them to produce more isotropic results.  represents a unit cell of the C₃S molecular structure and  represents a supercell of that same structure that is doubled on all three axes.

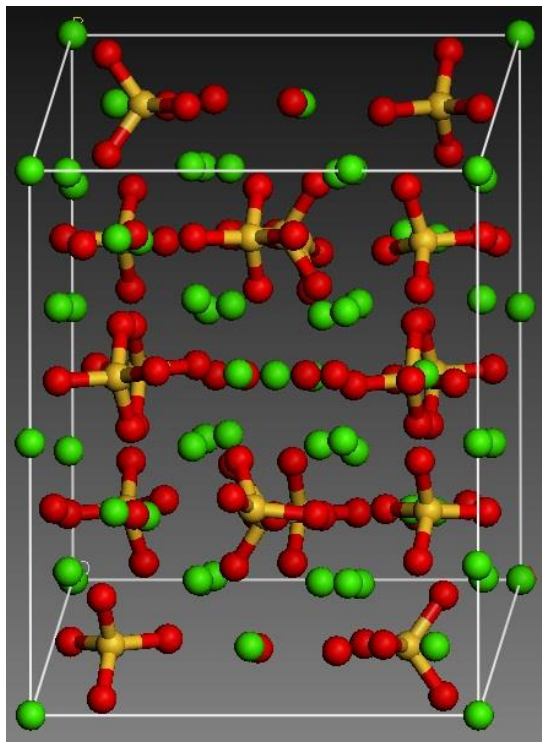


Figure 9: C₃S unit cell

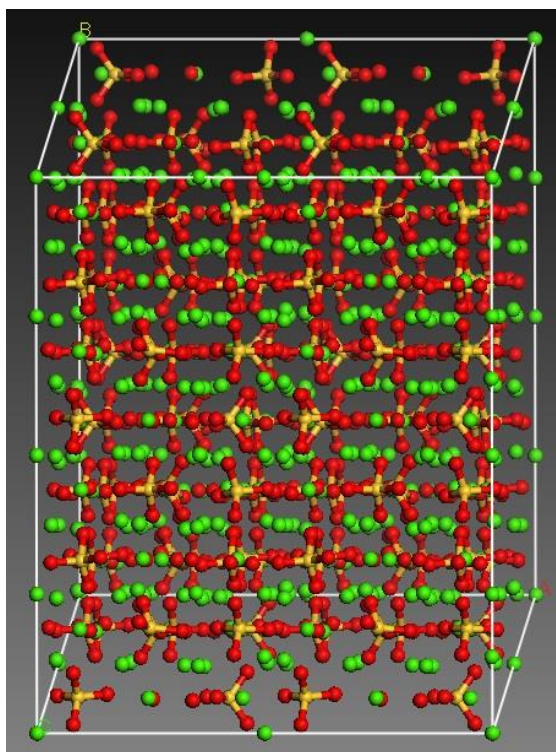


Figure 10: C₃S 2x2x2 Supercell

2.1.5. Effect of varying chain lengths

The mechanical properties of concrete can be greatly affected once it has been subjected to extreme environmental factors. Chemical and physical degradation occurs within the cement during certain environmental events, such as a prolonged or intense exposure to salts. MD tools can be used to study the mechanical properties and behavior of damaged C-S-H structures by changing the length of calcium silicate chains. In case study by Selvam et al., silicon chains are broken on a Tobermorite 11Å structure [Hamid, 1981] to create less stable unit cell structures with Ca/Si ratios of 1.25 and 0.83. As more Ca ions are removed from the structure, the potential energy of the system increases, becoming less negative. The cohesive energy of the atoms decreases as the potential energy increases, and an atom with a lower cohesive energy becomes energetically less stable [Selvam et al. 2009].

2.2. Input parameters

There is currently not a specific set of guidelines to follow for selecting input parameters for the mineral crystal structures used in this research for MD simulations. Therefore, when applying a thermodynamic ensemble, it is necessary to vary input parameters such as temperature, time step, and simulation time. The general starting point for the input parameters of a dynamics simulation is:

- Ensemble: NVT

- Temperature: 300K
- Thermostat parameter: 0.1 ps
- Equilibration time: 1.0 ps
- Production time: 50 ps
- Time step: 1.0 fs
- Number of steps: 50,000

If the results of the MD simulations are inadequate (i.e. high standard deviation of energies, negative values for elastic moduli, and etc.), the initial input parameters may need to be modified, the simulation may need to be repeated. If the standard deviation of the energy of the system is unreasonable, the time steps or total production time will need to be increased.

2.3. Effect of varying MD tools and forcefields

Several attempts are made at determining the best MD tool and forcefield combination for simulations of molecular cement models. Figure 11 displays the effect of using various MD tools and forcefields on a C-S-H molecular structure.

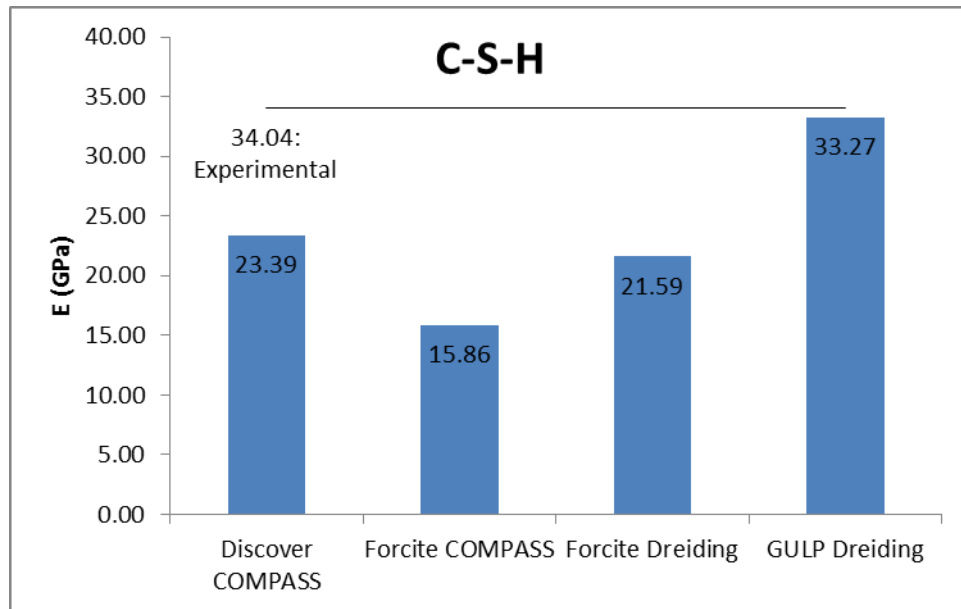


Figure 11: Effect of varying MD tools & forcefields with C-S-H model

The Discover-COMPASS and Forcite-Dreiding combinations produce results similar to those of Zhu et al. [2007] at 23.4 GPa and Constantinides et al. [2003] at 21.7 GPa, respectively.

However, these results are only for the LD C-S-H. The GULP-Dreiding combination provides results most closely resembling the nanoindentation testing results at 34.04 GPa.

2.4. Effect of varying cell sizes

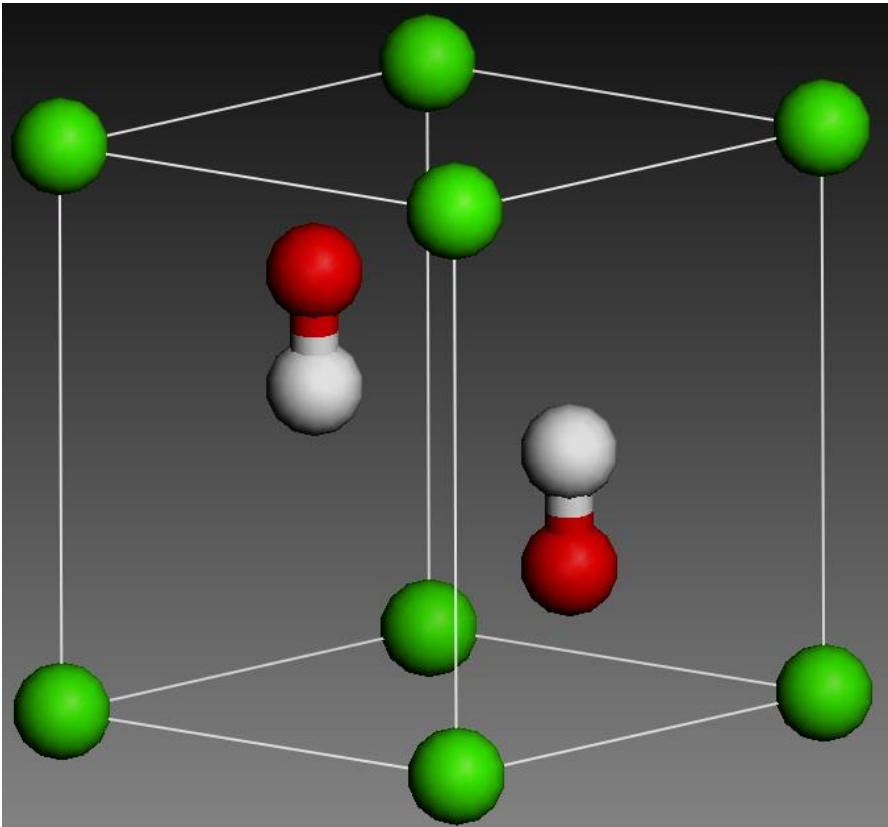
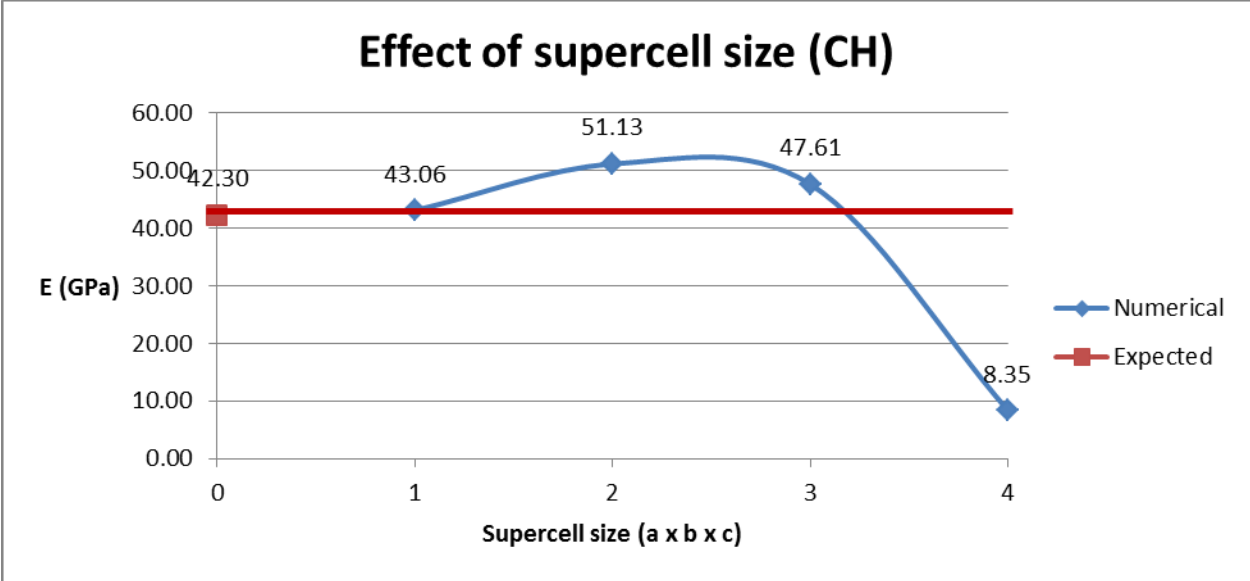


Figure 12: Calcium hydroxide unit cell

The calcium hydroxide structure used in this research was obtained through the American Mineralogist Crystal Structure Database filed under the mineral name “Portlandite.” The

structure was originally created by Henderson and Gutowsky [1962], and the cell parameters are listed below.

Table 2: Calcium hydroxide cell parameters

Type	CH		
	Density	Atoms	Volume
	2.26937	5	54.2160
Angle	α	β	γ
	90.0000	90.0000	120.0000
Length	A	B	C
	3.58500	3.58500	4.87100

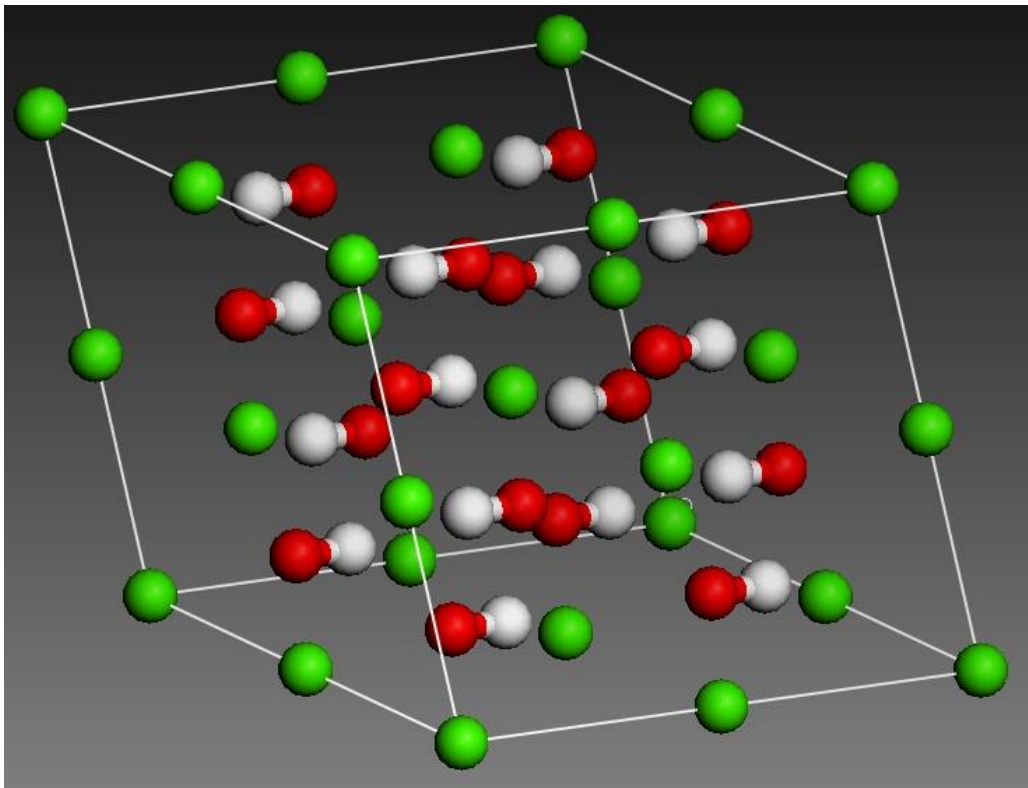


Figure 13: Calcium Hydroxide 2x2x2 Supercell

The 2x2x2 supercell of CH provides a more stable model by replicating the unit cell once in all three directions.

Table 3: Calcium hydroxide supercell parameters

Type	CH 2x2x2		
	Density	Atoms	Volume
	2.26937	40	433.728
Angle	α	β	γ
	90.0000	90.0000	120.0000
Length	A	B	C
	7.17000	7.17000	9.74200

2.5. Effect of varying chain lengths

The Tobermorite 11Å model by Hamid is modified by removing several calcium ions, representing deterioration, to create a model with a Ca/Si ratio of 1.25 and a model with a Ca/Si ratio of 0.83. All three of these models are compatible with only the GULP MD tool and the Dreiding forcefield (they are not compatible with the Discover or Forcite MD tools and there is not a compatible version of COMPASS that will operate within GULP).

Within the GULP MD tool, isotropic elastic properties are produced after an energy minimization is performed. However, after the molecular dynamics simulations have been performed, some of the C-S-H structures produce non-isotropic results which would require the application of a supercell.

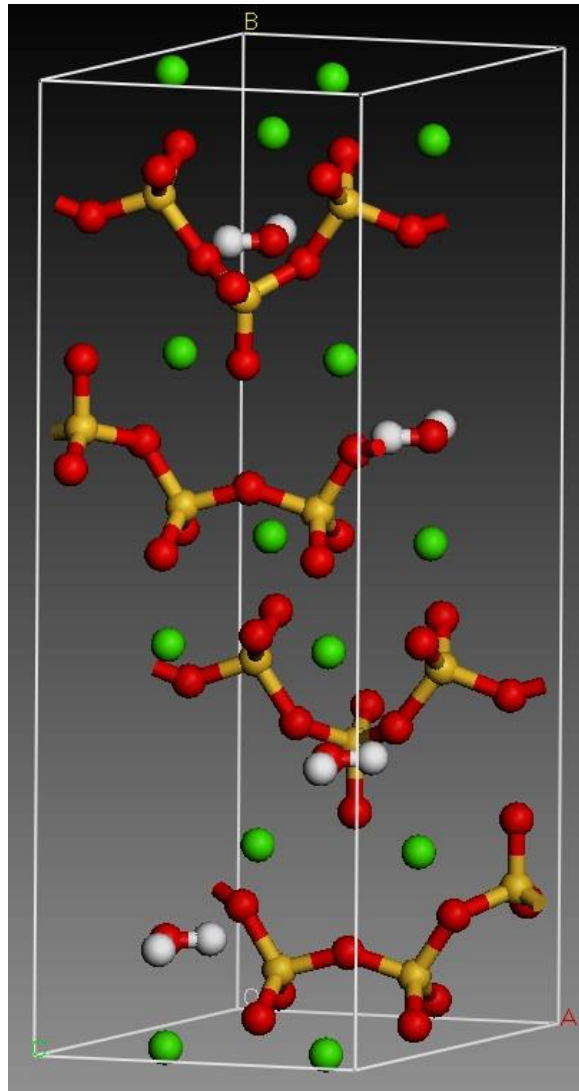


Figure 14: Tobermorite 11Å Chain with Ca/Si ratio 1.00

Figure 14 represents the full, original Tobermorite 11Å unit cell structure by Hamid which includes the complete amount of calcium ions. This structure is not compatible with the Discover and Forcite MD tools. Therefore, the GULP MD tool is the only available module within the Materials Studio MD software that will run a simulation on the Tobermorite 11Å by Hamid.

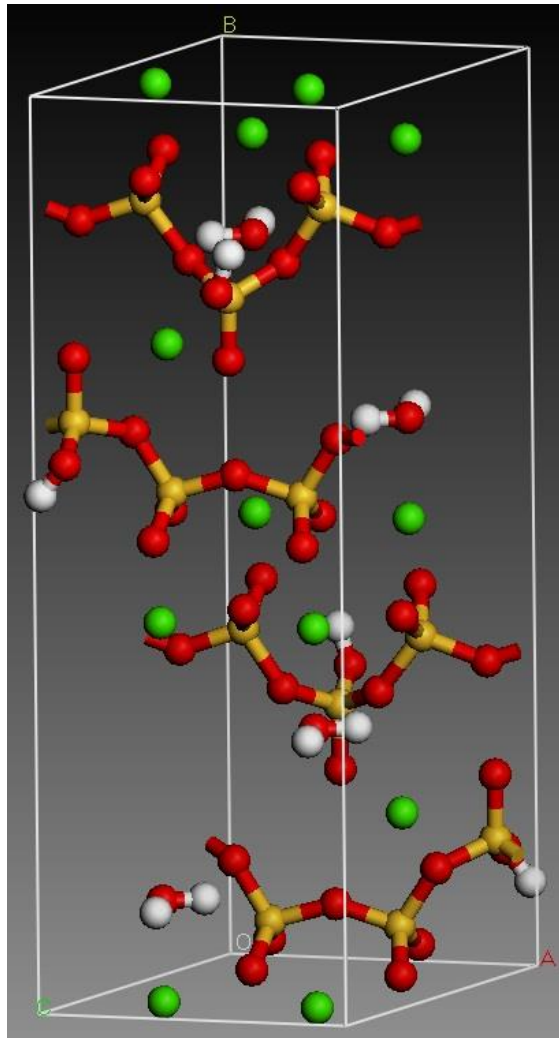


Figure 15: Tobermorite 11Å Chain with Ca/Si ratio 0.83

The unit cell represented in Figure 15 is a modified version of the Tobermorite 11Å structure with several silicon chains broken to mimic damage upon the structure. The ends of the broken bonds are capped with hydrogen ions, resulting in a Ca/Si ratio of 0.83.

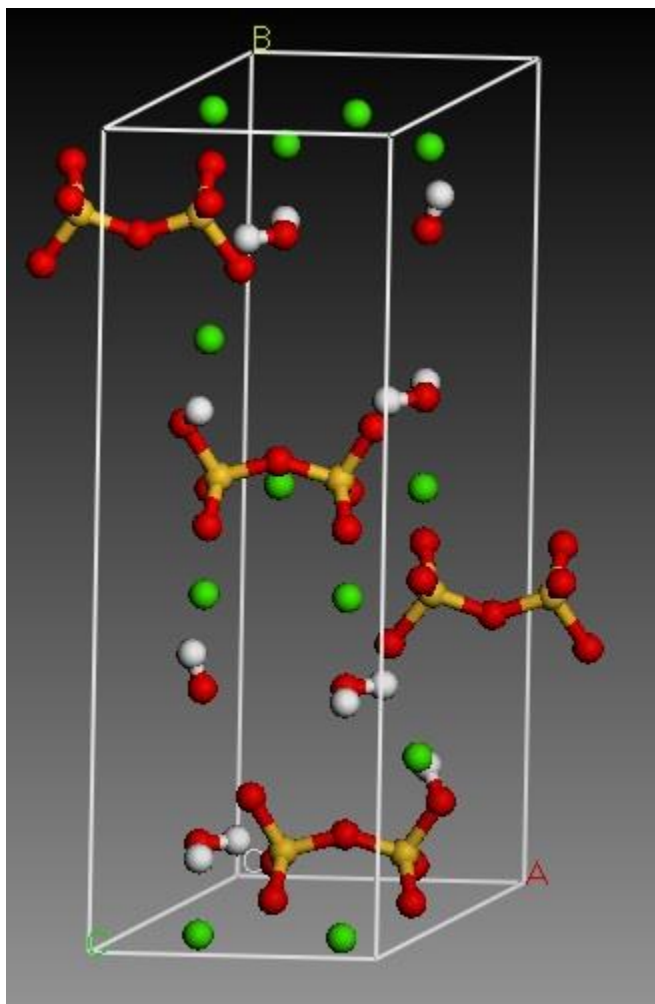


Figure 16: Tobermorite 11Å Chain with Ca/Si ratio 1.25

The unit cell represented in Figure 16 is also a modified version of the Tobermorite 11Å structure with several silicon chains broken, resulting in a Ca/Si ratio of 1.25. The ends of the broken bonds of this structure are also capped with hydrogen ions.

1.25

Figure 17: MD simulation on the effect of chain length

The results shown in Figure 17 represent the effect of modifying the chain the length of the Tobermorite 11Å model. The elastic modulus of the complete structure is 61.78 GPa, and as more chains are broken to Ca/Si ratios of 0.83 and 1.25, the modulus decreases to 26.92 GPa and 35.75 GPa, respectively. This could be due to extra rigidity provided by the addition of extra hydrogen ions which would be similar to extended hydration of Portland cement in the real world.

3. Experimental

The experimental portion of this research includes the physical testing of hardened Portland cement paste and hardened C_3S paste through atomic force microscopy and nanoindentation testing. Also included in this section is the x-ray powder diffraction of C_3S .

3.1. Nano cement manufacturing

Nano-C-S-H is created by hydrating C_3S that was manufactured in the Nano Infrastructure Modeling Laboratory at the Jackson Avenue Center. The components of C_3S are displayed in Table 4. These components are synthesized by dissolving the solid particles in water and mixing the solution by hand using a metal spatula. The solution is further mixed using a magnetic stirring apparatus to form a homogeneous solution. This solution is heated to 100°C for thirty minutes until a paste is formed. That paste is then placed in a high-heat ceramic dish and annealed at 1000°C for thirty minutes which allows the particles to crystallize and form the desired nano-cement component. After cooling, the nano-cement is ground down into a fine powder using a mortar and pestle and then placed in a sealed container to protect it from moisture (which could lead to undesired hydration). At that point, it is ready for analysis through X-ray diffraction and the hydration process.

Table 4: C_3S Components

C_3S Components	Amount (by weight)
Polyethylene glycol (PEG)	35 g
$\text{Ca}(\text{C}_2\text{H}_3\text{O}_2)_2$	47 g

SiO ₂	29 g
H ₂ O	150 g

Challenges have arisen during the hydration process of the manufactured C₃S. A typical water-cement ratio (0.45) is used at first, but C₃S powder with this amount of water fails to form a paste. Therefore, water is added to separate samples to create water-cement ratios of 0.60, 0.80, 1.00, 1.20, and 1.40. The hydrated C₃S does not form a paste resembling cement until it is mixed with w/c ratio of 1.20 or more (see Figure 18 and Figure 19). These specimens are given 36 hours to set. The hardened C₃S samples are then placed in a bath of water to cure for 7-10 days. Samples with w/c ratios greater than 1.40 break apart and dissipate in the water during the curing process.

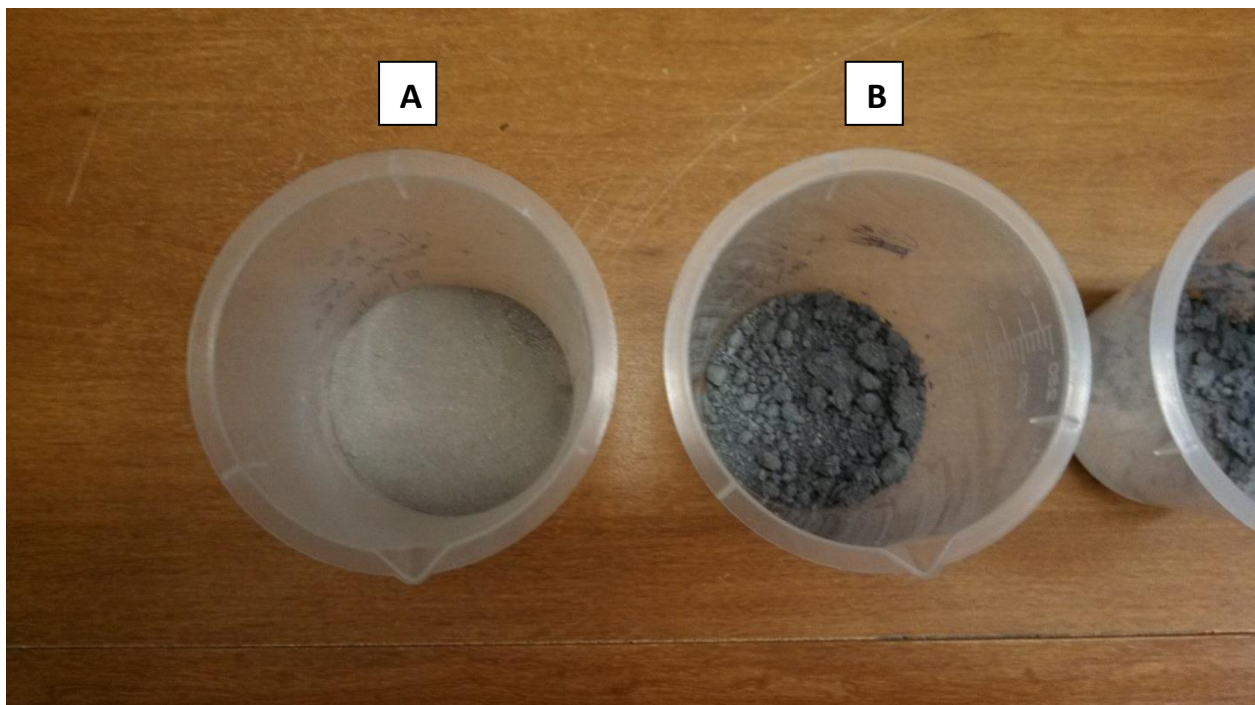


Figure 18: A. C₃S with w/c ratio 0.60, B. C₃S with w/c ratio 0.80

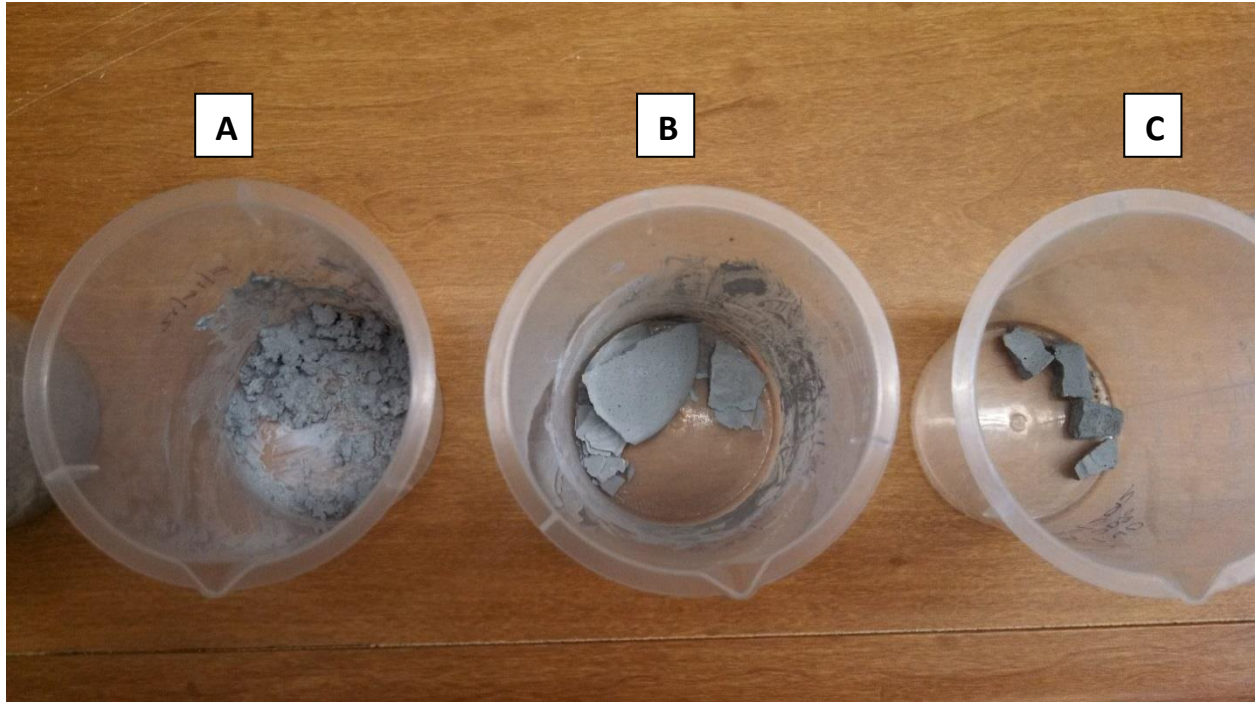


Figure 19: A. C_3S with w/c ratio 1.00, B. C_3S with w/c ratio 1.20, C. C_3S with w/c ratio 1.40

3.2. XRD

Procedure

A sample of C_3S that has been ground into a powder is placed in the Bruker D8 Powder XRD Instrument at the National Center of Physical Acoustics in University, MS (see Figure 20). An X-Ray beam is blasted through the sample which produced a spectrum that was computed through the computer software for the machine. The 2θ range is from 10° to 80° . The peaks in the spectrum can then be compared to the C_3S spectrums on the mineralogy website and literature to confirm that the specimen was pure C_3S [American]. The same procedure is repeated for a sample of hardened Portland cement paste that has been crushed and ground into a powder.



Figure 20: Bruker D8 Powder X-Ray Diffractometer at NCPA

XRD spectrum results

The C_3S requires validation through X-ray powder diffraction after each batch of specimens has been created. The output spectrum from the powder diffraction scans are compared to the spectrums from the American Mineralogist online mineral database [American] or a spectrum produced by the Reflex module in the commercially available software Materials Studio. The Reflex module produces a spectrum based on a molecular structure that has been created in the Materials Studio 3D Atomistic Visualizer.

Figure 21 represents a comparison between the XRD spectrum of C_3S executed at the NCPA (bottom) and a C_3S spectrum established in the literature by Lin et al. [1997] (top). Major peaks match at 2θ equal to approximately 29° , 32° , and 34° .

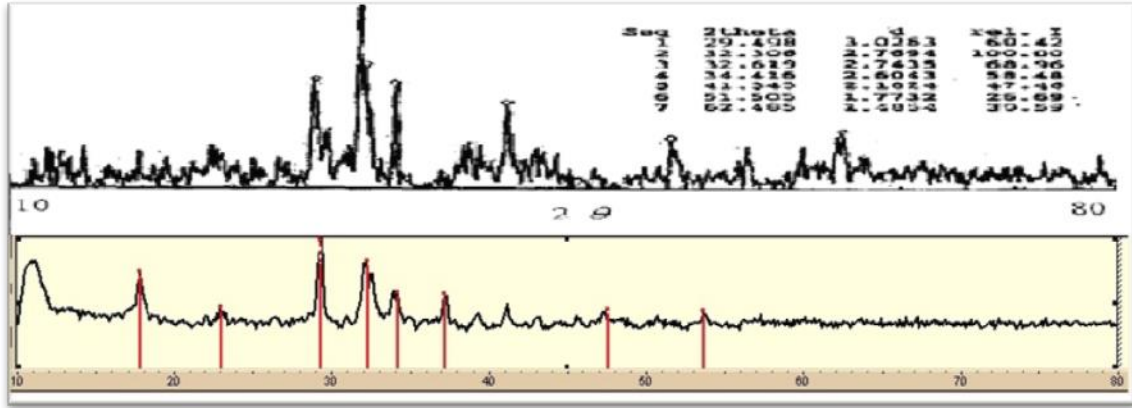


Figure 21: Top: C₃S XRD Spectrum from literature; Bottom: C₃S XRD spectrum from experiment

Hardened Portland cement paste (w/c: 0.45) is crushed into a fine powder suitable enough for XRD at the NCPA, and the results are represented in the bottom portion of Figure 22. The resulting spectrum is compared to the spectrum in the top of Figure 22 where three peaks are matched that represent a presence of portlandite (CH) and small presence of ettringite (CS).

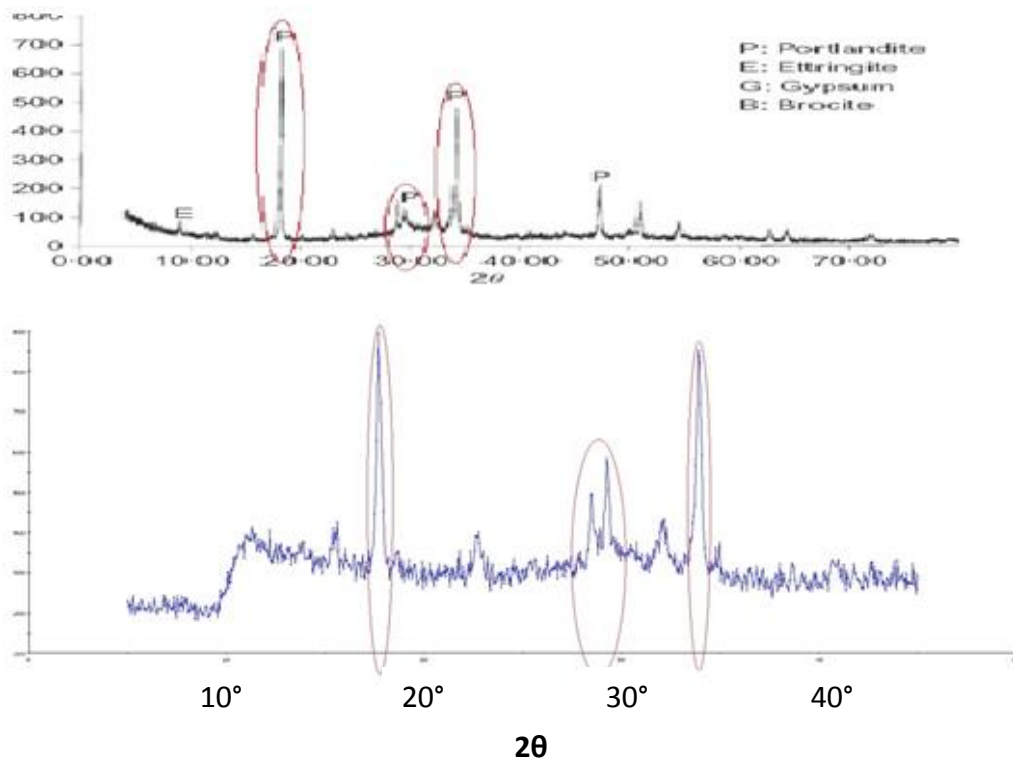


Figure 22: Top: HCP XRD Spectrum from literature; Bottom: HCP XRD spectrum from experiment

3.3. Sample preparation



Figure 23: Buehler Grinding/Polishing Table

Due to the extremely high-resolution of AFM, proper preparation of a sample is very important. It is very important to have an extremely smooth surface for examination through AFM imaging, otherwise, images will not be clear and important information will not be visible (see Figure 23). The tips used are very small (5-60 nm radius of curvature) so, a poorly polished sample will produce a poor image. Also, the nano-tips are susceptible to breaking when coming in contact with a rough surface. The samples must be polished in multiple stages of decreasing grit size.

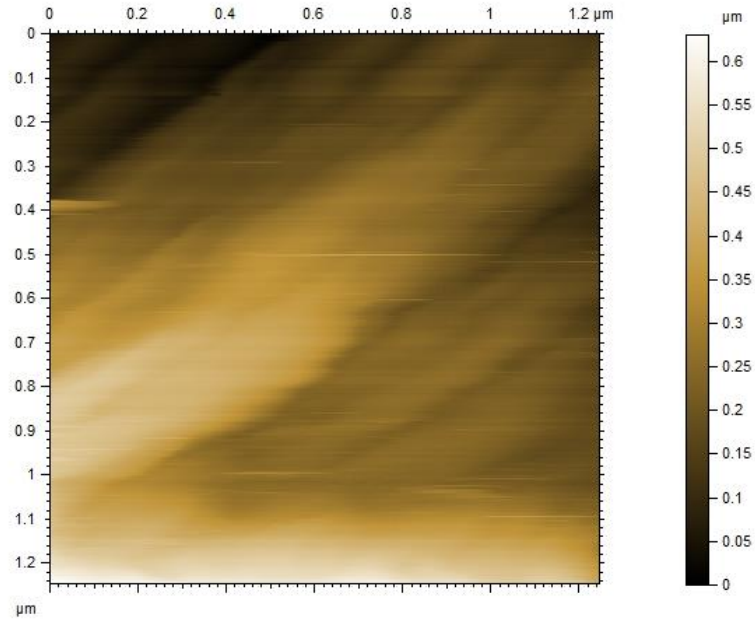


Figure 24: AFM image of a poorly polished cement sample

Much like AFM, it is important to have an extremely smooth and flat surface to produce accurate nanoindentation results. For nanoindentation, it is important that the sample surface is not only smooth, but it must also be flat. During a nanoindentation mapping test, the indenter must move from one indent location to the next unobstructed, and, if a sample is not mounted flat and level, false readings will be recorded or the tip could become damaged (see Figure 24).

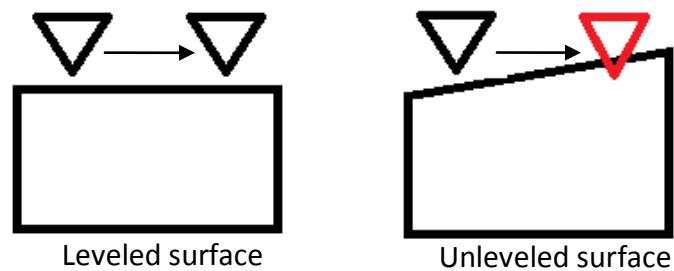


Figure 25: Unobstructed vs. obstructed nanoindenter tip paths

Ideally, nanoindentation tests should produce a curve similar to the one represented in Figure 23. However, a poorly polished Portland cement specimen will produce hysteresis curves like those represented in Figure 26 and Figure 27. In Figure 26, as the Berkovich tip is being unloaded from the surface of the sample, the unloading portion of the hysteresis curve behaves erratically and is not smooth. Figure 27 is an experimental representation of Figure 23. In this case, the Berkovich tip is touching the surface of the specimen before the load cell has begun recording the load for the test. As it unloads, the unloading portion of the hysteresis curve is above the loading curve and continues past the point of initial loading. In other words, the initial loading of the curve occurred in the plastic deformation zone and the nanoindenter recorded the depth after indentation to be less than the depth of the initial indentation. A specimen that has been properly prepared and is flat will not produce an ideal hysteresis curve similar to Figure 5.

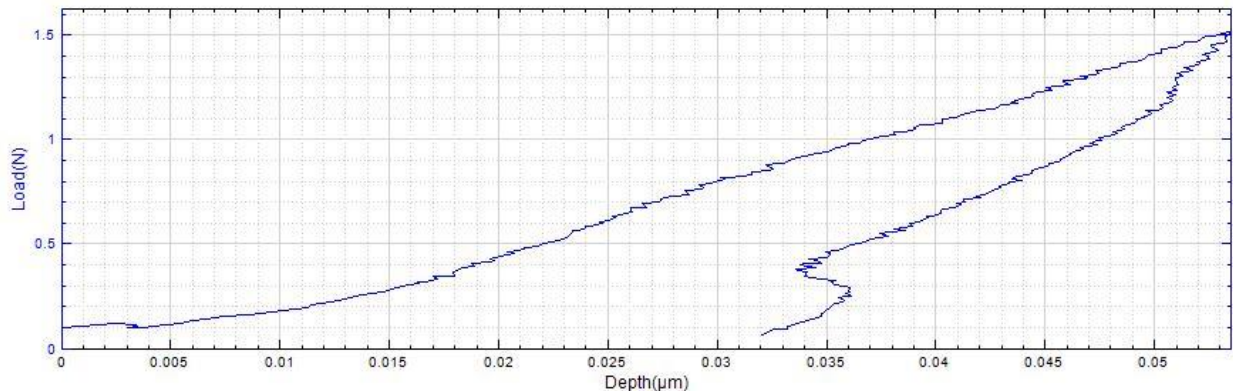


Figure 26: Nanoindentation test of a poorly polished Portland cement specimen at a max applied load of 1.5 mN

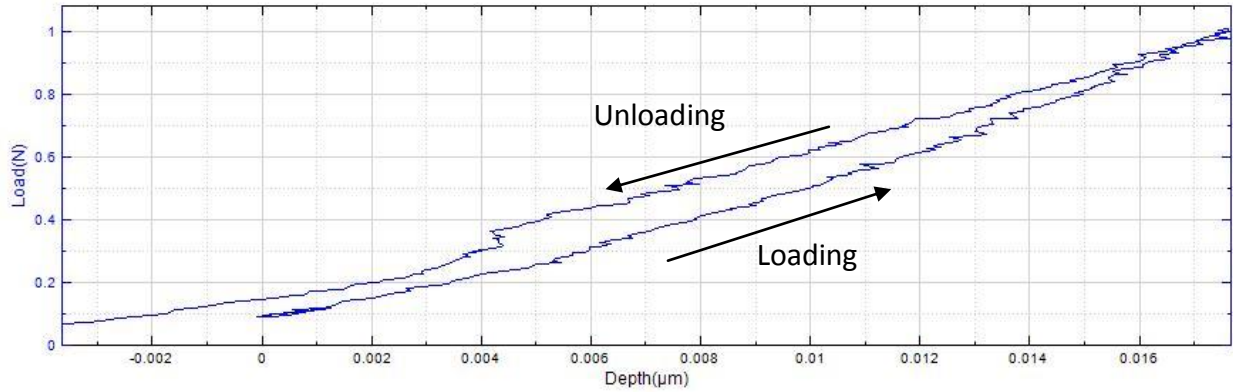


Figure 27: Nanoindentation test of a poorly polished Portland cement specimen at a max applied load of 1 mN

Sample preparation at NIRG laboratory

Proper polishing of the samples is critical. A polishing table with interchangeable sandpaper pads (see Figure 23) is used to polish all samples with polishing pads of various grit sizes. The samples were wet-sanded, meaning, as the polishing pads spun on the table, water or alcohol was applied to the surface to keep the temperature of the sample down. Samples were polished at gradually increasing sandpaper grit fineness: P240 (58.5 μm particle diameter), P400 (35.0 μm particle diameter), and P800 (21.8 μm particle diameter).

Sample preparation at ERDC

Another variation of a sample preparation is performed at the Engineer Research and Development Center (ERDC) of the US Army Corps of Engineers in Vicksburg, MS. The researchers and engineers at ERDC place great emphasis on their thorough sample polishing technique. It is a multiple-stage process that is fairly time consuming if it is performed properly. The samples are mounted to aluminum cylinders (diameter: 1.25" and height: 0.75")

using crystalbond. To prevent further or undesired hydration of the cementitious materials, ethylene glycol is used instead of water to lubricate and keep the temperature of the samples from rising during polishing. Also, to prevent further hydration, these samples are submerged in ethanol instead of water during sonication. Sonication is performed after each stage in polishing for approximately 8 minutes to remove any residue from polishing. Initially, sonication of the cement samples was performed for a minimum of 10 minutes, but the water became hot which caused the crystalbond to become loose and eventually settle on the recently-polished surface of the samples. So, sonication time is reduced to approximately 8 minutes. After sonication is performed, the sample must be placed under an optical microscope to be examined for scratch sizes. If a scratch is found on the surface of the specimen that is larger than the particle size of the sandpaper used in the previous step, grinding must continue on that same paper. Once the scratch size is smaller than the particle size of the sandpaper, grinding and polishing can begin on the next sandpaper grit size.

3.3.1. ERDC Sample preparation procedure

1. *Mold type should be made of non-absorbent material, 1.25" in diameter*
2. *Coat the interior of the mold with a releasing agent*
3. *Place the sample at the bottom of the mold and ensure that no particles are left under the sample*
4. *Mix the epoxy product following the Standard Operating Procedures from Buehler*
5. *Remove the sample from the mold without striking or damaging the surface*
6. *Mark the non-surface with an ID*
7. *Use a Sharpie to create a ring on the circumference of the cured epoxy*

3.3.2. ERDC Grinding/polishing procedure

1. *Use ethylene glycol as grinding lubricant*
2. *2 minute grind – use 240 grit paper (53.0 micron particle size) until Sharpie line is removed*
3. *4 minute grind – use 400 grit paper (23.0 micron particle size)*
4. *8 minute grind – use 600 grit paper (16.0 micron particle size)*
5. *12 minute grind – use 1200 grit paper (6.5 micron particle size)*
6. *Flush the surface with ethanol in a squeeze*
7. *Switch over to a diamond or aluminum suspension*
8. *Use a polishing lubricant with 50:50 combination of:*
 - a. *Ethylene glycol*
 - b. *Ethanol*
9. *15 minute polish – use 6 micron aluminum suspension*
 - a. *Spray with Ethanol*
10. *15 minute polish – use 0.3 micron aluminum suspension*
 - a. *Spray with Ethanol*
11. *15 minute polish – use 0.05 micron diamond suspension*
 - a. *Spray with Ethanol*

3.4. Atomic Force Microscopy

3.4.1. Procedure

After the sample is properly prepared, it may be imaged with the AFM. This procedure begins with placing the sample in the microscope and then inserting the appropriate scanning tip (tapping mode tip or contact mode tip). The laser in the AFM is calibrated to comply with the properties of the nano-tip inserted in the previous step. The computer software is then opened. Within the software, scan size, scanning mode, and other variables are inputted to provide the software with the necessary information for generating the desired image.

AFM images of hardened Portland cement paste

The AFM images acquired of hardened Portland cement paste provide evidence of multiple phases within the C-S-H structure. Figure 28 reveals the presence of two types of C-S-H, HD C-S-H and LD C-S-H, throughout the scan area. LD C-S-H and HD C-S-H are identified by recognizing the packing of the 5.6 nm globules similar to those represented in Figure 1

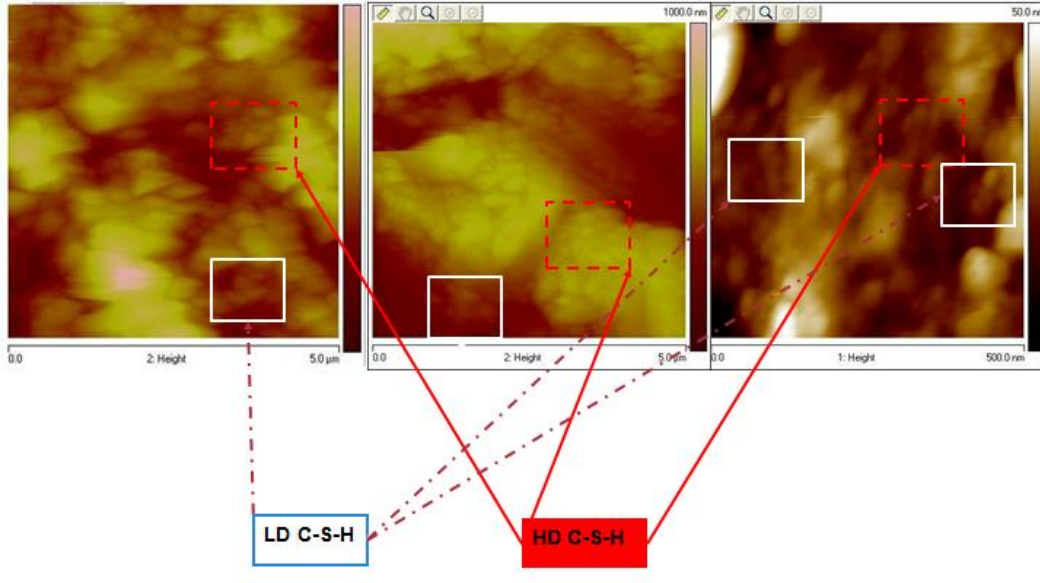
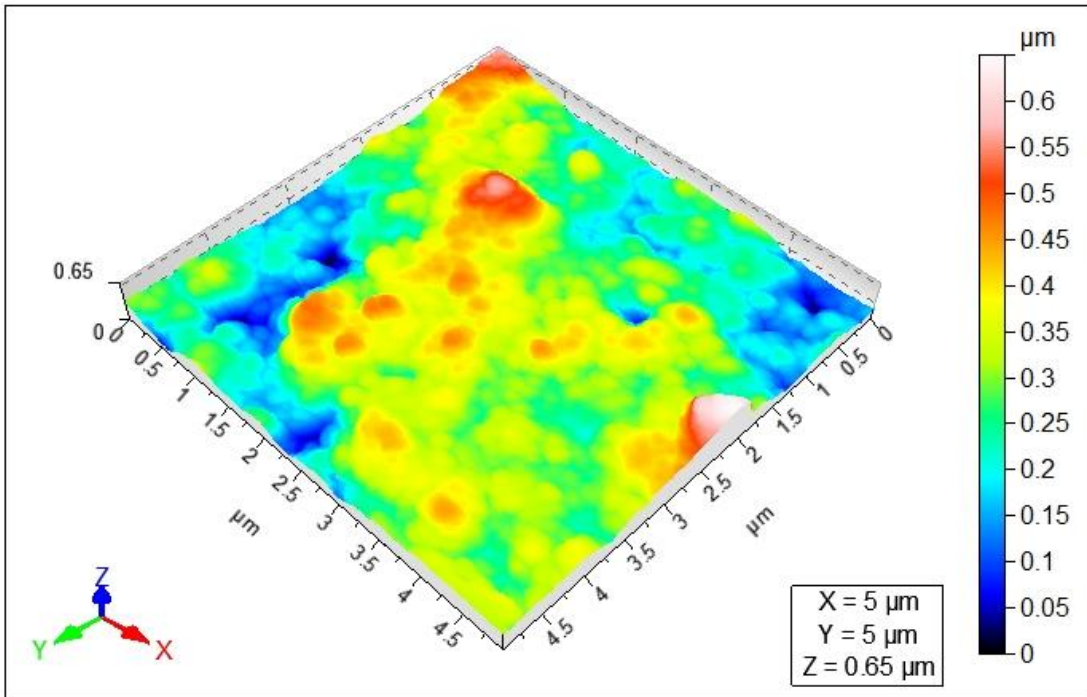
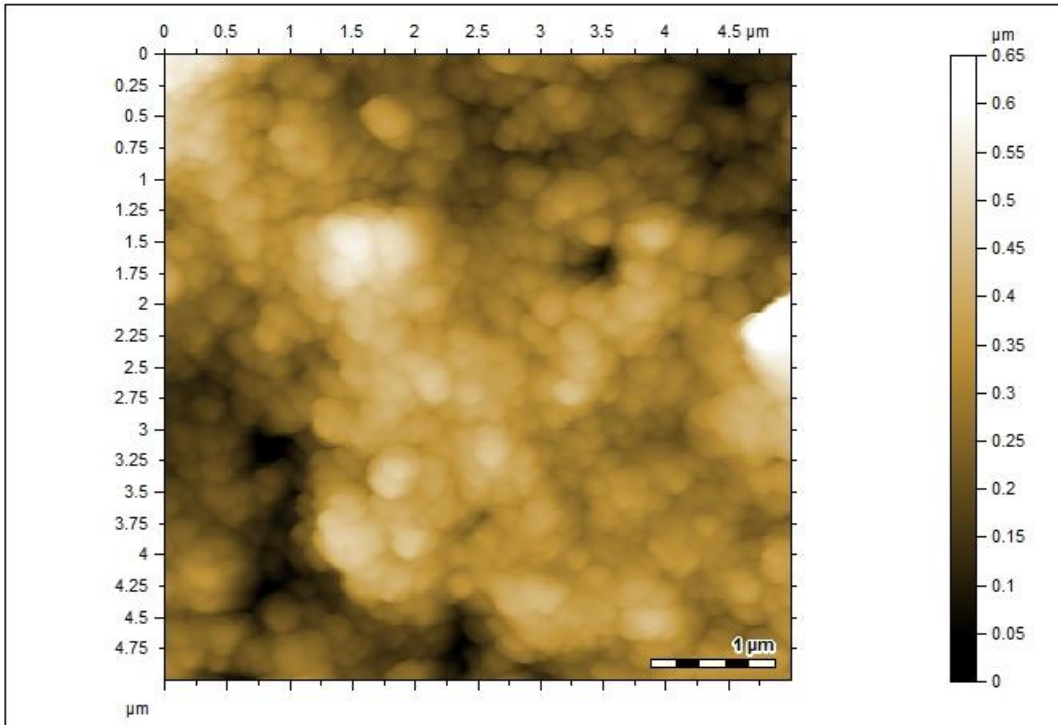


Figure 28: AFM of hardened Portland cement paste with phase ID

Portland Cement - Height Image



Expert 3D 6.2.6409

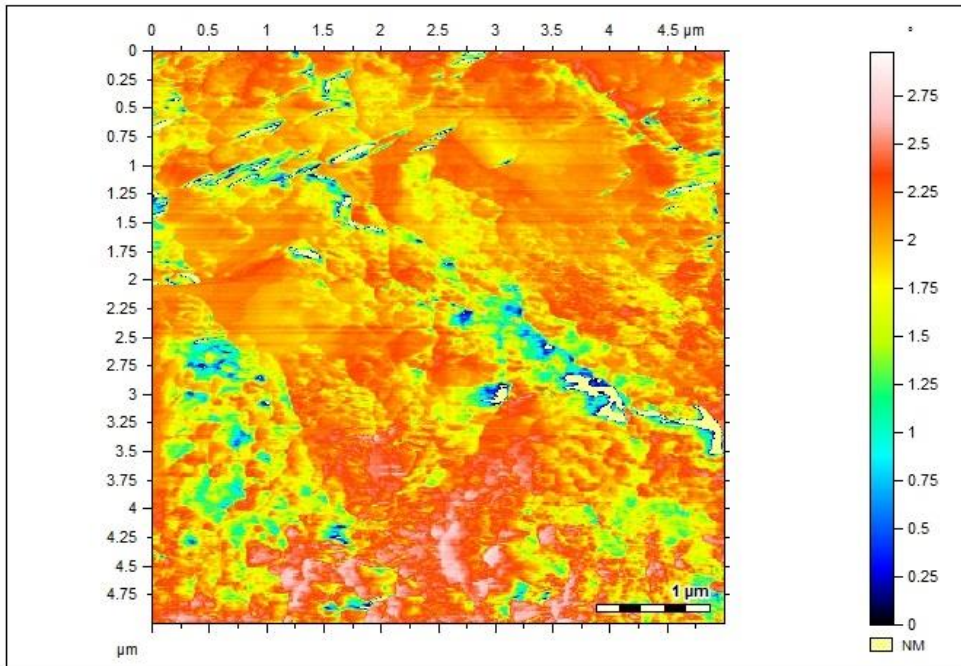
Figure 29: Portland cement topographic image and 3D image

An AFM scan that has been cleaned and modified using MountainMaps is represented in Figure 29. In this topographic image, a Portland cement specimen with a scan size of 5 microns has been fine-tuned to make the image appear crisper. Also, a 3D effect has been placed on the image to give a better idea of the height changes in the topography.

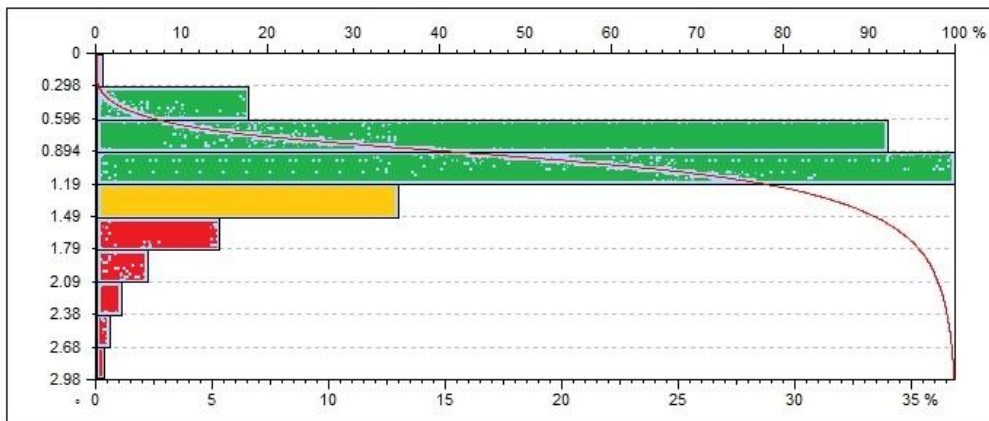
3.4.2. Phase analysis

The phase contrast images can provide information of the composition of the Portland cement specimen that has been scanned. With the MountainMaps software, frequency distribution plots can be created based on the phase contrast images. Results from MD simulations, XRD spectrum analyses, and NI histogram quantifications provide a basis for a correlation with the AFM phase contrast histograms. For example, an XRD spectrum analysis for hardened Portland cement paste identifies approximately 70% C-S-H and CH. This value can be identified on the phase contrast histogram and correlated with the phase angle to show where these components appear on the image. Similarly, the percentages of the distribution of cementitious components identified from NI histograms can be imposed on the AFM phase contrast histograms showing the amount of each component on the AFM phase contrast image.

Portland Cement - Phase Image



Phase Frequency Distribution



C-S-H & CH: approx. 77%

Unreacted clinker: approx. 10%

CS: approx. 13%

Figure 30: Phase contrast image and histogram of Portland cement (5 micron scan size)

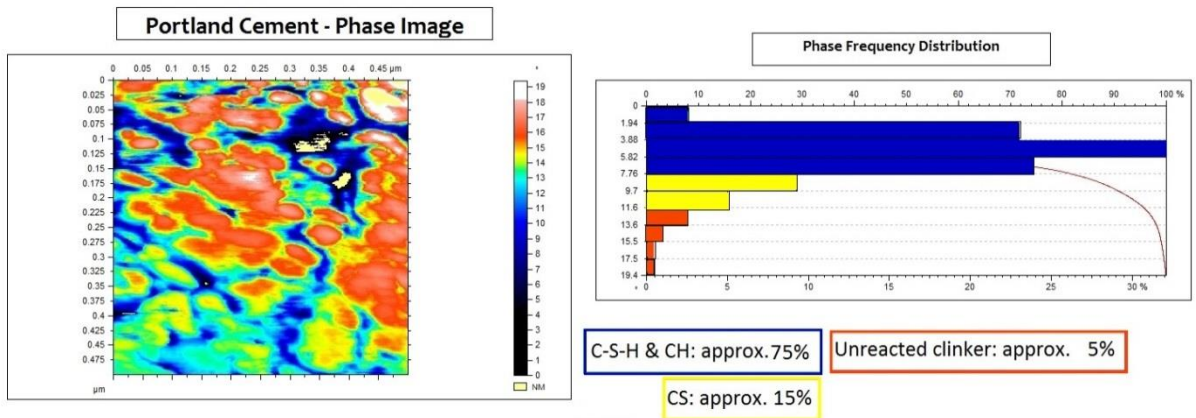
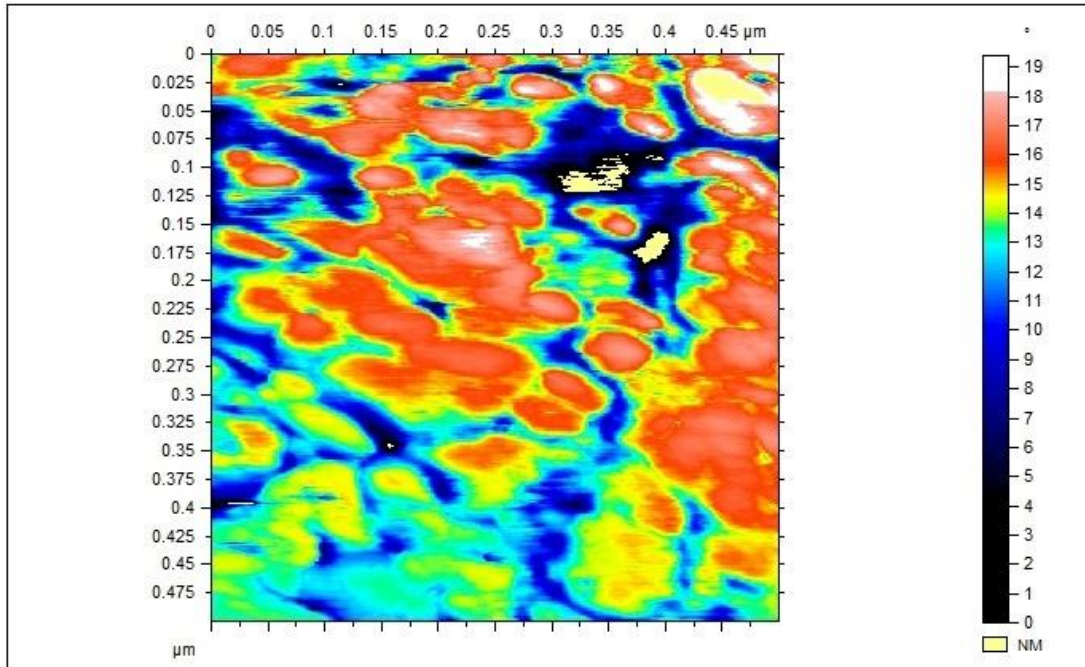
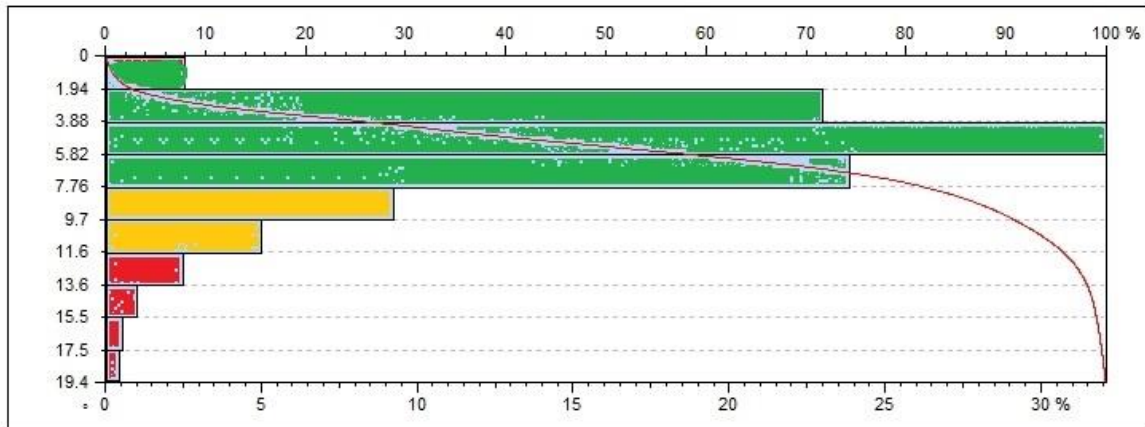


Figure 31: Phase contrast image and histogram of Portland cement (500 nm scan size)

Portland Cement - Phase Image



Phase Frequency Distribution



C-S-H & CH: approx. 75%

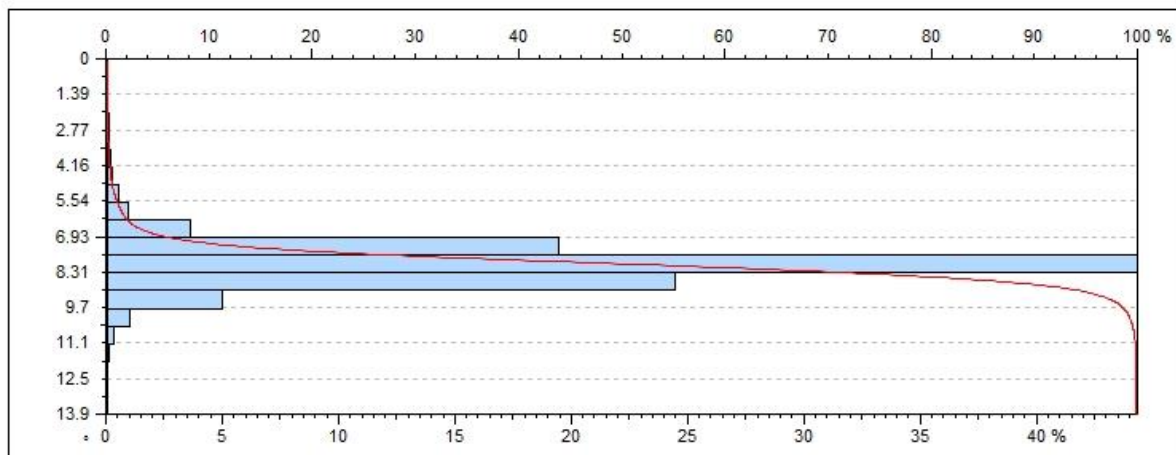
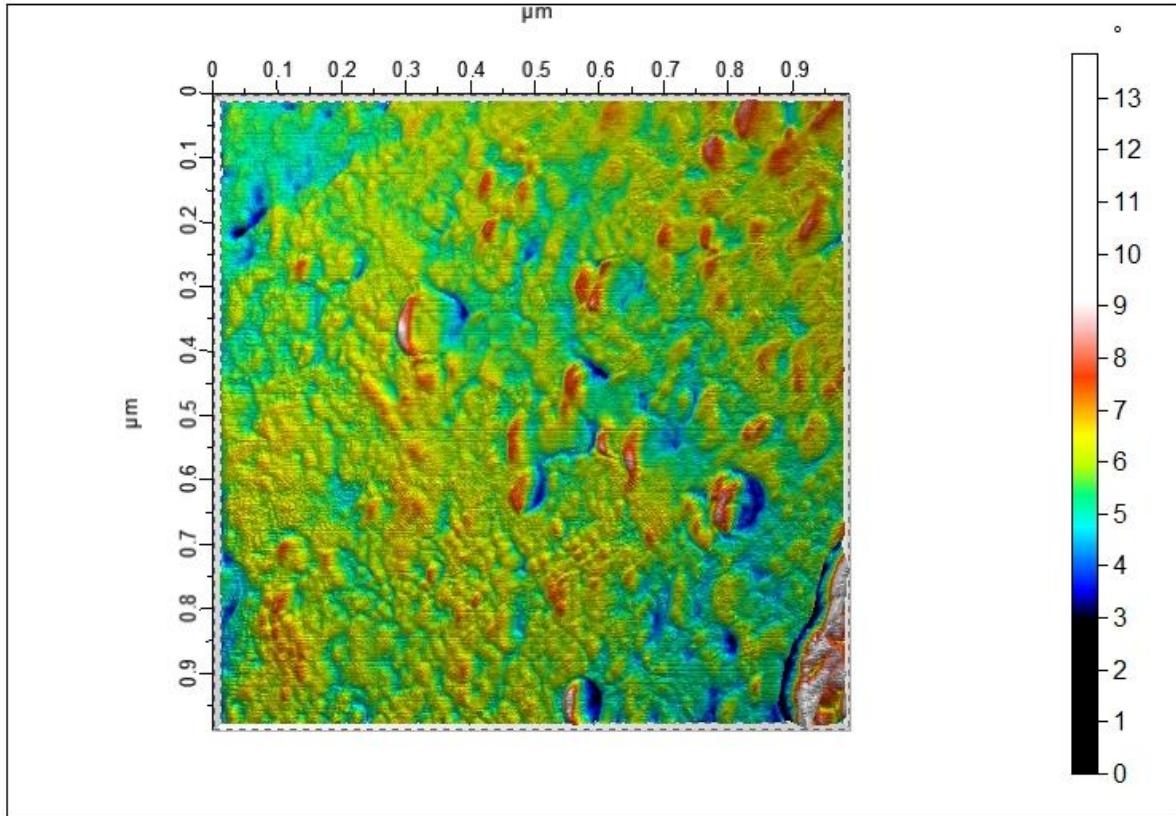
Unreacted clinker: approx. 5%

CS: approx. 15%

Expert 3D 6.2.6409

Figure 32: Phase contrast image and histogram of Portland cement (500 nm scan size)

Portland Cement - Phase



Expert 3D 6.2.6409

Figure 33: Phase distribution of hardened Portland cement paste (1 micron scan size)

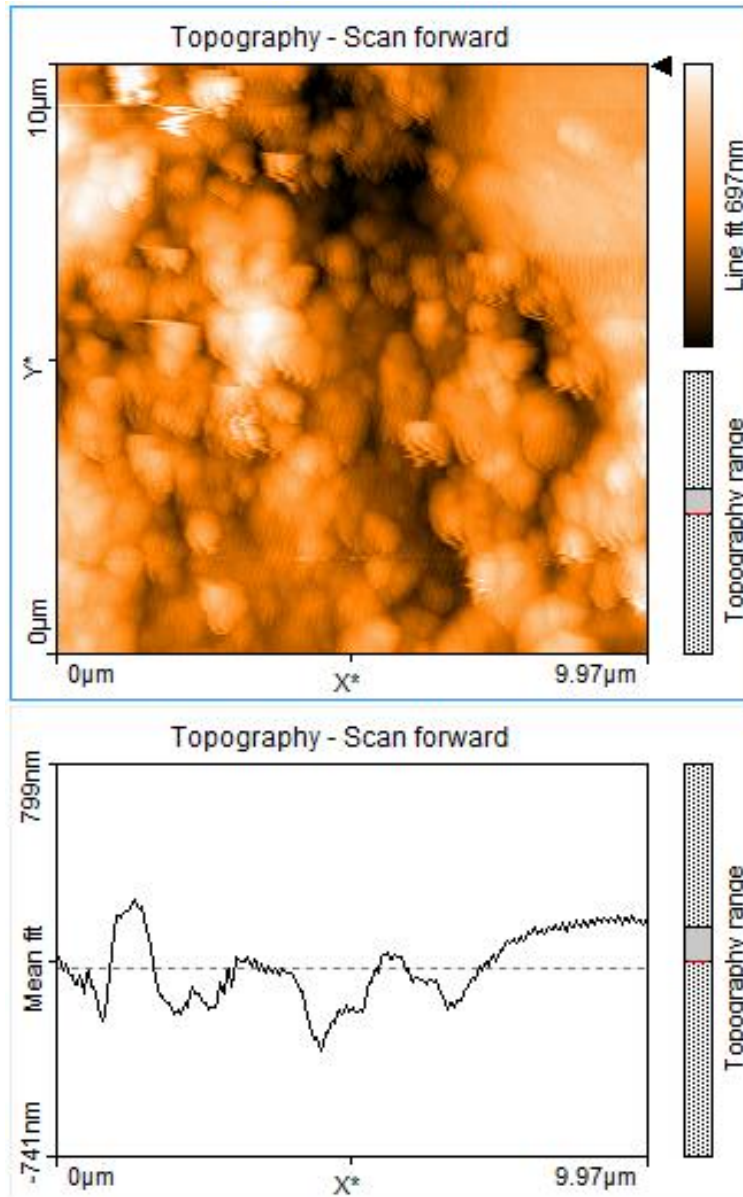


Figure 34: AFM image of cement from Nanovea AFM (10 micron scan size)

An example of a poor AFM image is represented in Figure 57. Even though some globules can be distinguished from this image, there is a large presence of noise.

3.5. Nanoindentation

3.5.1. Procedure

Once they are thoroughly polished, samples can be loaded into the nanoindenter and testing can begin. The Portland cement is analyzed by loading and unloading the Berkovich tip on the surface of the specimen multiple times on a predetermined grid (map, Figure 31). Initially, the cement samples are tested using a maximum load of 25 mN, loading at a rate of 50 mN/min with a grid of 4x10. Various maximum applied loads are later tested and described in further detail in the following section.

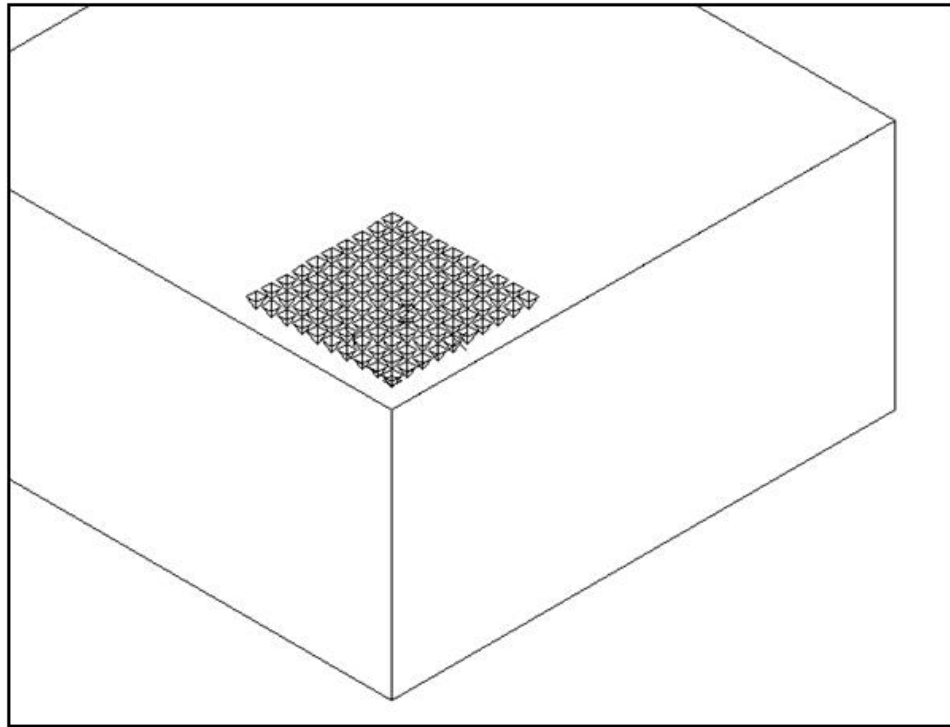


Figure 35: 10x10 Nanoindentation mapping

3.5.2. Effect of Loading

Varying the maximum applied load of the nanoindentation produces different mechanical properties. Papers by Němeček (2012), Yao et al. (2013), and Constantinides et al. (2006) suggest that maximum applied force for nanoindentation of cementitious materials should be no more than 2 mN. The highest average elastic moduli of Portland cement are recorded during tests in which the maximum applied loads are between 1.5 mN and 10 mN. When the maximum applied load is higher than 10 mN, the elastic modulus gradually begins to decrease (see Figure 36).

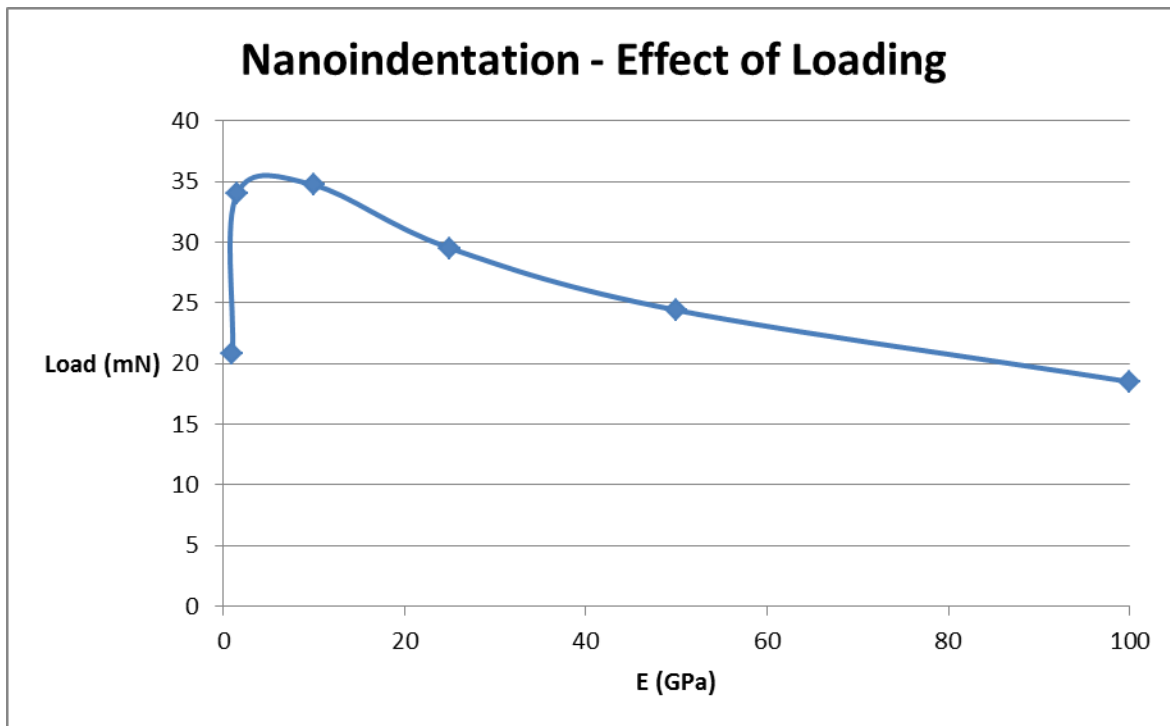


Figure 36: Effect of varying the maximum applied load in nanoindentation tests on Portland cement

Load (mN)	E (GPa)	# of indents
1	20.8	39
1.5	34	66
10	34.7	150
25	29.5	99
50	24.4	150
100	18.5	60

Table 5: Effect of varying the maximum applied load in nanoindentation tests

3.5.3. Nanoindentation of hardened Portland cement paste

A sample of unhydrated Type I/II Portland cement powder is mixed with deionized water at a w/c ratio of 0.45 and left to set for 24 hours. After 24 hours has passed, the sample is placed in a bath of deionized water to cure for seven days. Once, curing is complete, the sample is prepared for nanoindentation using the polishing technique described in Section 2.2.3. A specimen of hardened cement paste that is ready for nanoindentation will look similar to the specimen in Figure 37.



Figure 37: Hardened Portland cement paste specimen ready for nanoindentation

The prepped cement specimen is placed on the stage of the nanoindentation unit, and the optical microscope is utilized to determine a desired location on which the nanoindentation tests are to be performed. The stage of the nanoindentation unit delivers the specimen to the nanoindenter and places the selected area directly underneath the Berkovich tip. After many trials of various maximum loads (see Section 3.5.2), a maximum applied load of 1.5 mN is chosen for a nanoindentation test with a grid of 5 x 15 (75 indentations). There are 9 indentations that generate hysteresis curves in which mechanical properties cannot be obtained, leaving 66 curves to be analyzed.

Type I/II Portland Cement Nanoindentation Results

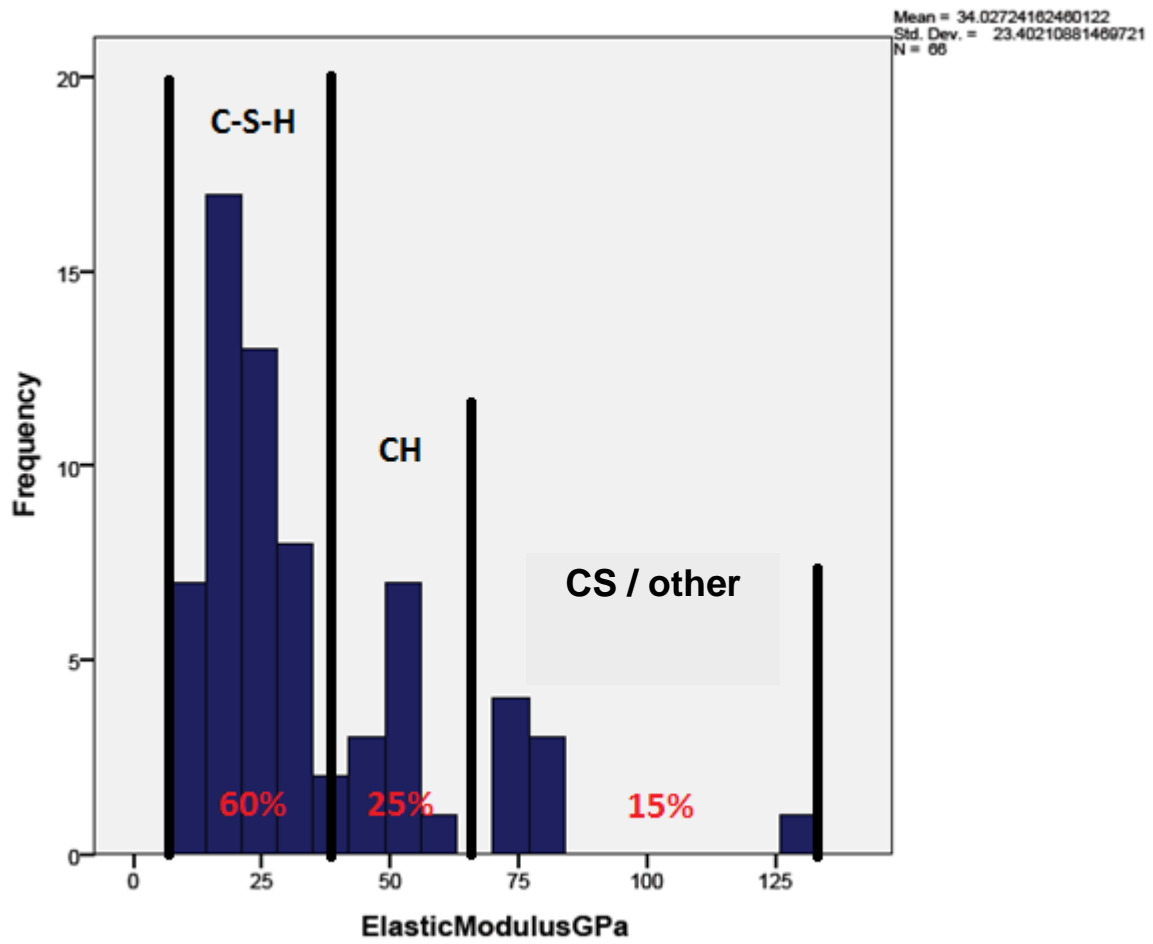


Figure 38: Nanoindentation of cement phase distribution histogram

Portland cement frequency distribution

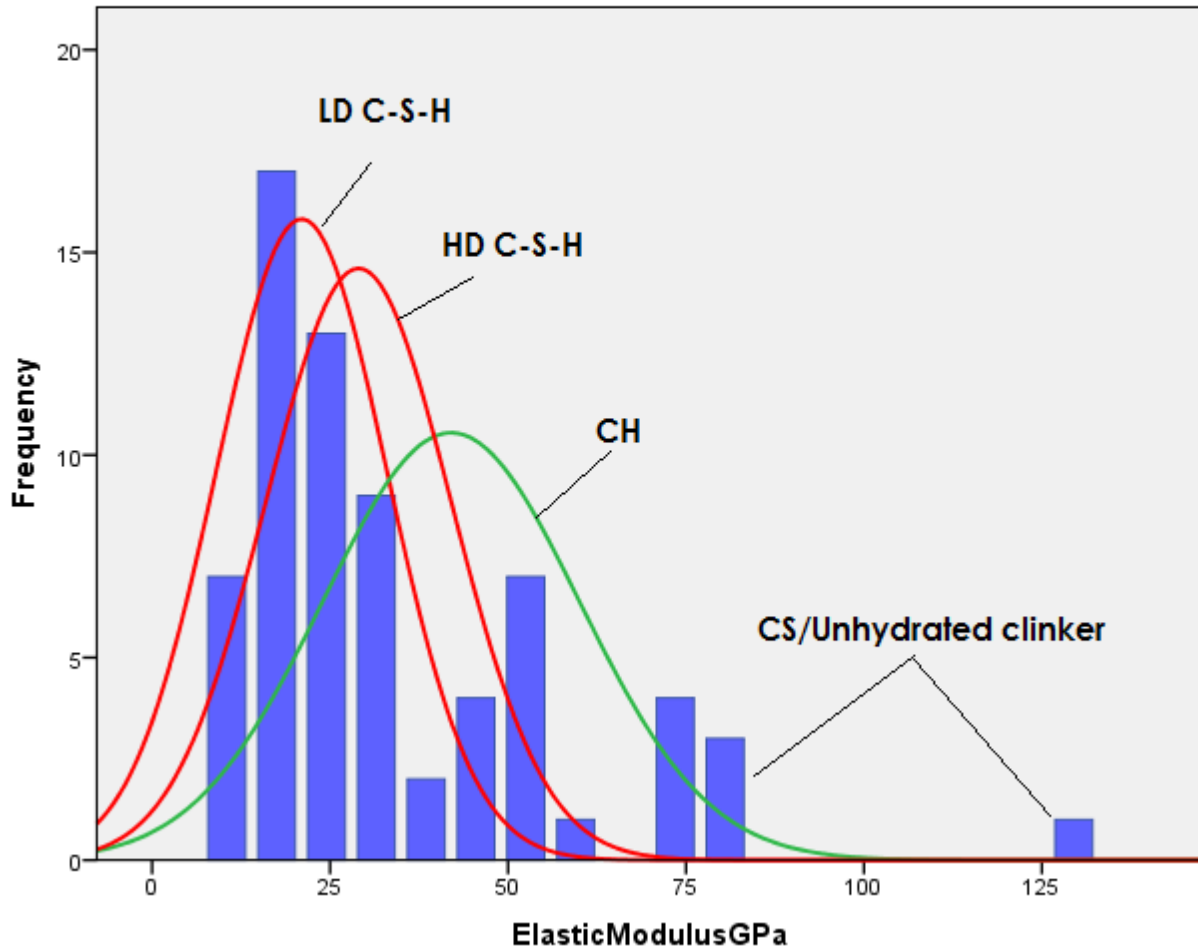


Figure 39: Frequency distribution of elastic moduli of Portland cement nanoindentation

The distribution of the frequency of the elastic moduli represented in Figure 38 and Figure 39 show evidence of the presence of the hydrated cement components in the hardened Portland cement paste specimen. The range of elastic moduli that closely resemble the results from MD simulations of C-S-H represents approximately 60% of the distribution. Similarly, the range of elastic moduli most closely resembling the MD results of CH represents approximately 25% of

the distribution. The remaining values are expected to be calcium sulfo-aluminate (ettringite) and other unhydrated minerals.

The hysteresis curves shown in Figure 40 represent indentations that result in elastic moduli ranging from 15 GPa to 35 GPa. These elastic properties fall in a range that can be associated with C-S-H. The maximum indentation depths for this group of hysteresis curves range from approximately 0.21 microns to 0.52 microns (with an exception of one curve with a maximum depth of 0.71 microns).

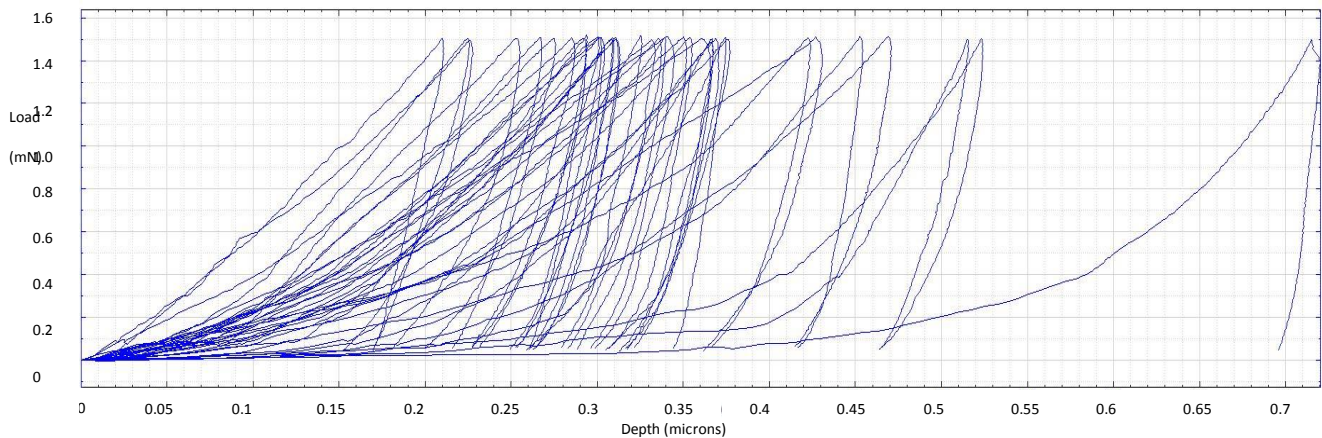


Figure 40: Hysteresis curves of C-S-H (from 15-35 GPa)

The hysteresis curves shown in Figure 41 represent indentations that result in elastic moduli ranging from 35 GPa to 60 GPa. These elastic properties fall in a range that can be associated with CH. The maximum indentation depths for this group of hysteresis curves range from approximately 0.16 microns to 0.35 microns.

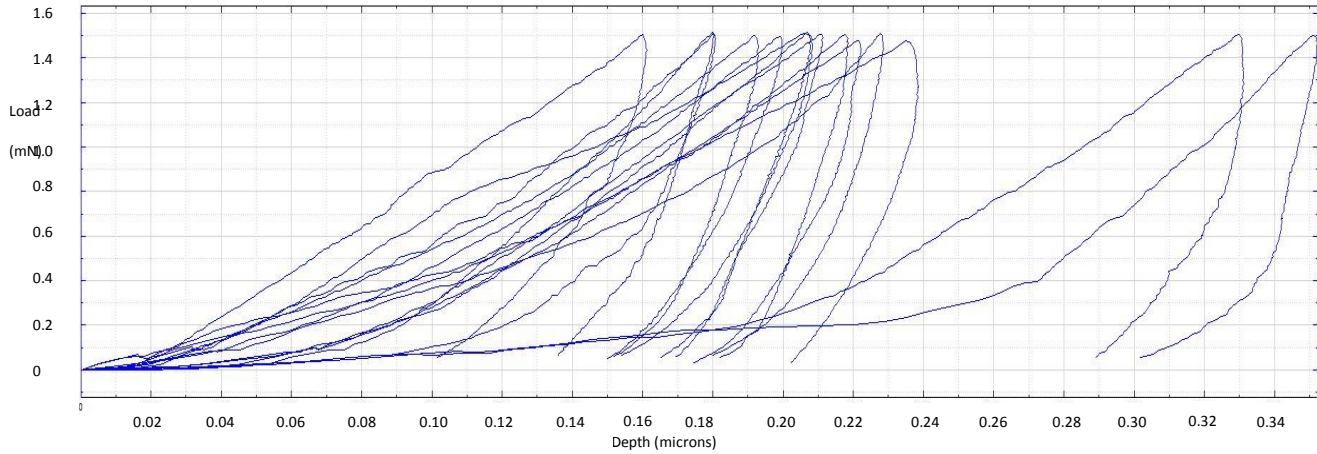


Figure 41: Hysteresis curves of CH (from 35-60 GPa)

The hysteresis curves shown in Figure 42 represent indentations that result in elastic moduli from two ranges: 0 to 15 GPa and 60 GPa and above. These elastic properties do not fall in a range that can be associated with either C-S-H or CH, and they are assumed to be other materials within the Portland cement. The maximum indentation depths for these groups of hysteresis curves range from approximately 0.11 microns to 0.22 microns for the stronger group and 0.37 microns to 0.69 microns for the weaker group.

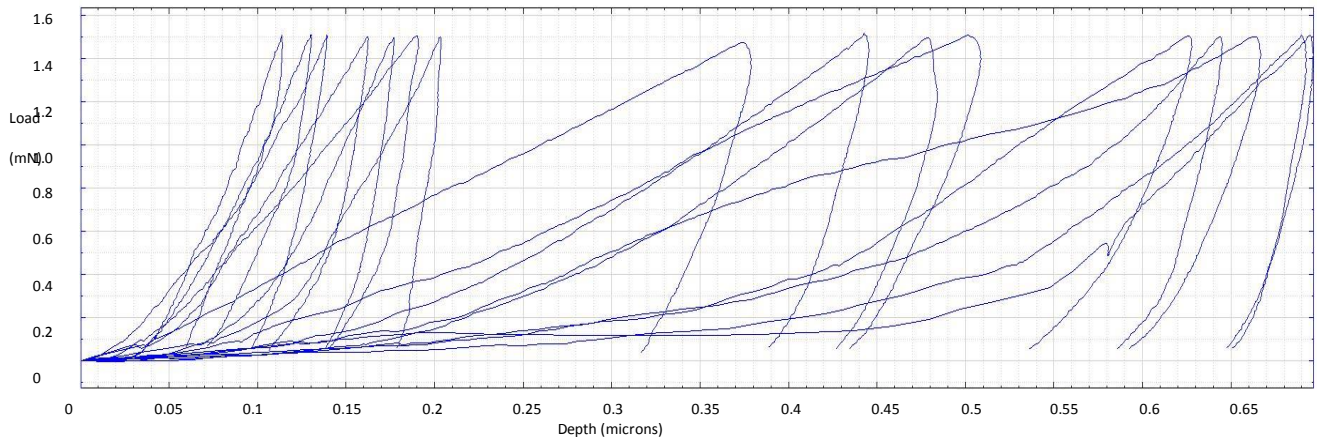


Figure 42: Hysteresis curves of other materials in Portland cement (0-15 GPa and 60-max GPa)

3.5.4. Nanoindentation of C₃S

A C₃S sample with a w/c ratio of 1.20 is cured for 7 days at 45°C before it is prepared for nanoindentation testing. The specimen is prepared in the Nano Infrastructure Research Laboratory (NIRL) at the University of Mississippi using the procedure described in With this amount of grinding and polishing, nanoindentation testing results reveal that C₃S (w/c: 1.20) has an elastic modulus equal to approximately 20.7 GPa. In an attempt to reduce the w/c ratio, the C₃S powder is mixed with Type I/II Portland cement at a 3:1 ratio and a w/c ratio of 1.00. Another sample is prepared similarly except with the addition of 5% gypsum. The results are presented in Figure 43.

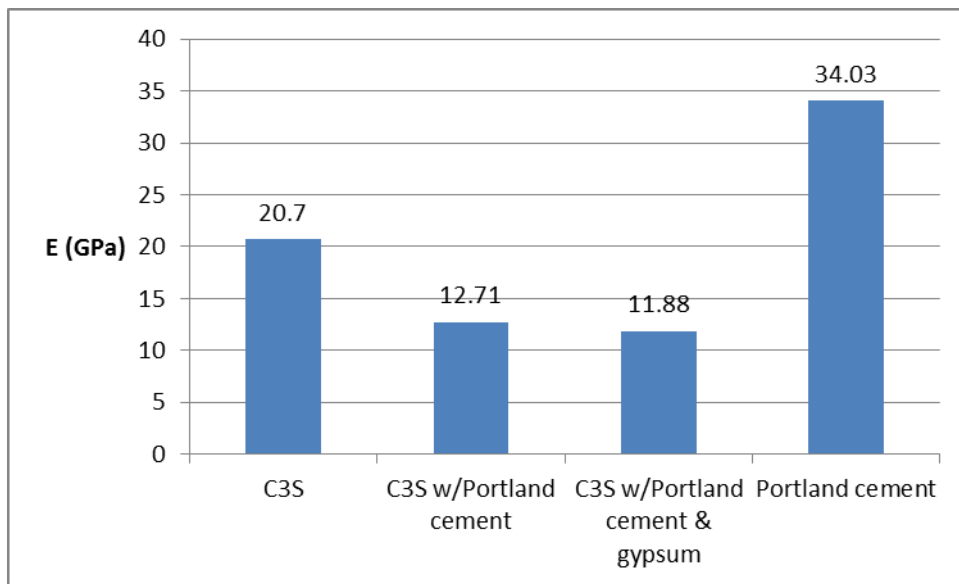


Figure 43: Nanoindentation results of hydrated C₃S and cement

The specimen is then polished using the technique used by the scientists at ERDC (see Figure 44) which is described in Section. However, once this specimen has met the ERDC standards,

another set of nanoindentation tests are performed on the specimen, resulting in an average elastic modulus of 30.9 GPa, which is closer to that of hardened Portland cement paste.



Figure 44: C₃S (w/c: 1.20) after preparation at ERDC

1 mN Loading

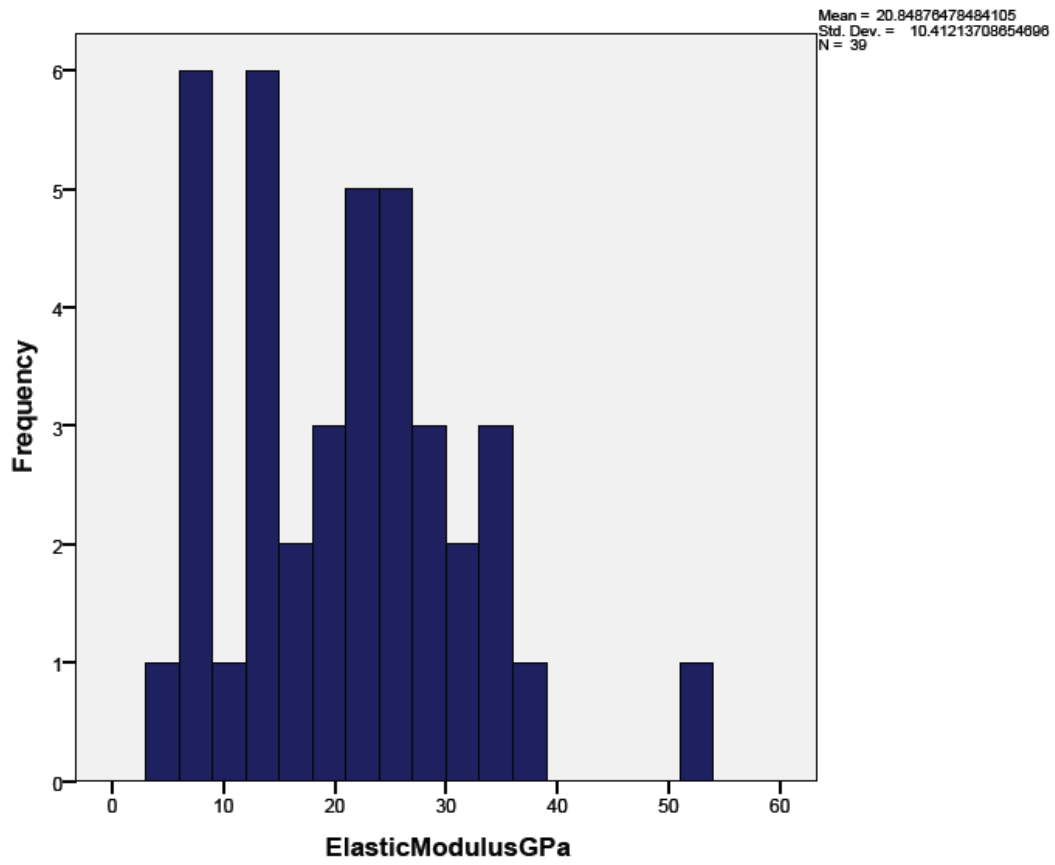


Figure 45: Frequency of elastic moduli of Portland cement with 1 mN max applied load

is the histogram of a nanoindentation test performed on hardened Portland cement paste with a maximum applied load of 1 mN. The average modulus of elasticity of this test is 20.9 GPa which is less than the test with the maximum applied load of 1.5 mN and the well-established modulus of Portland cement.

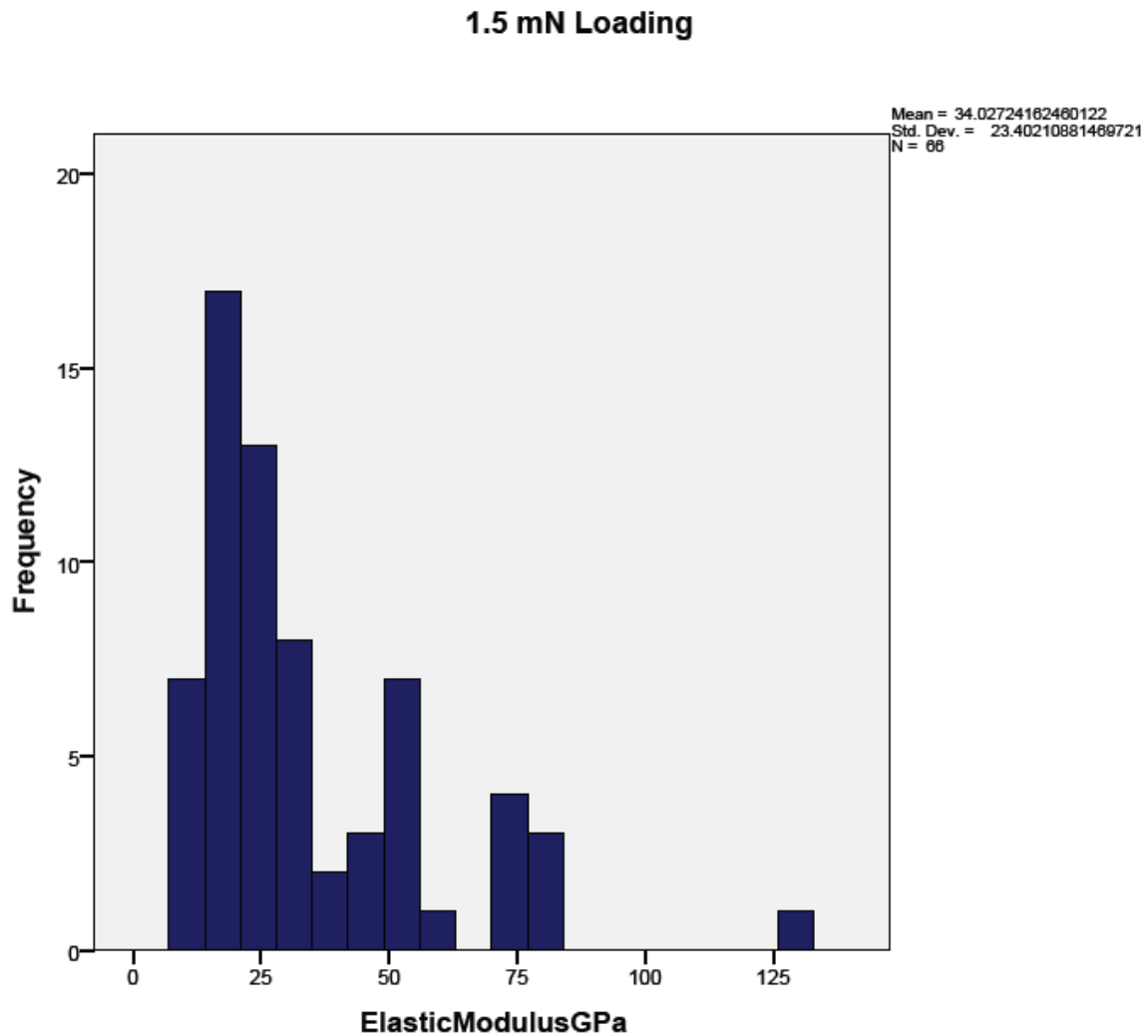


Figure 46: Frequency of elastic moduli of Portland cement with 1.5 mN max applied load

10mN Loading

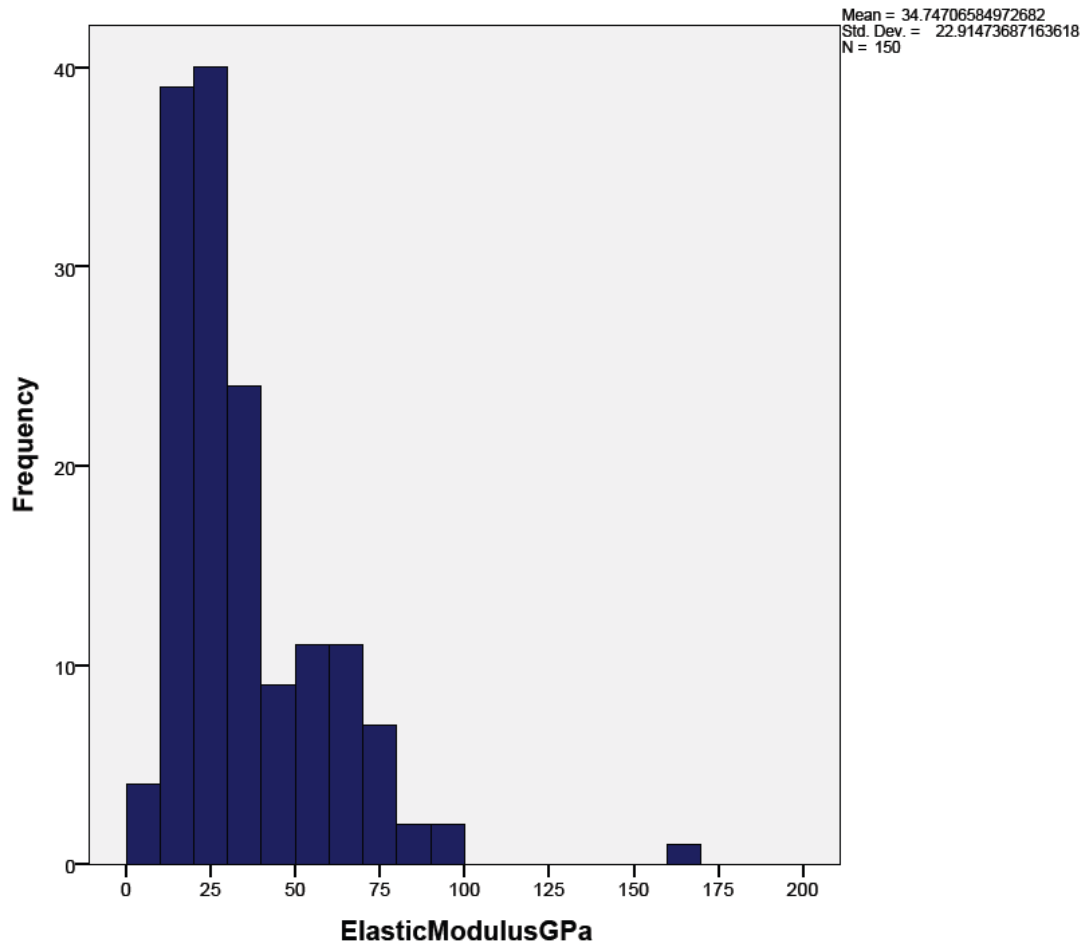


Figure 47: Frequency of elastic moduli of Portland cement with 10 mN max applied load

50mN Loading

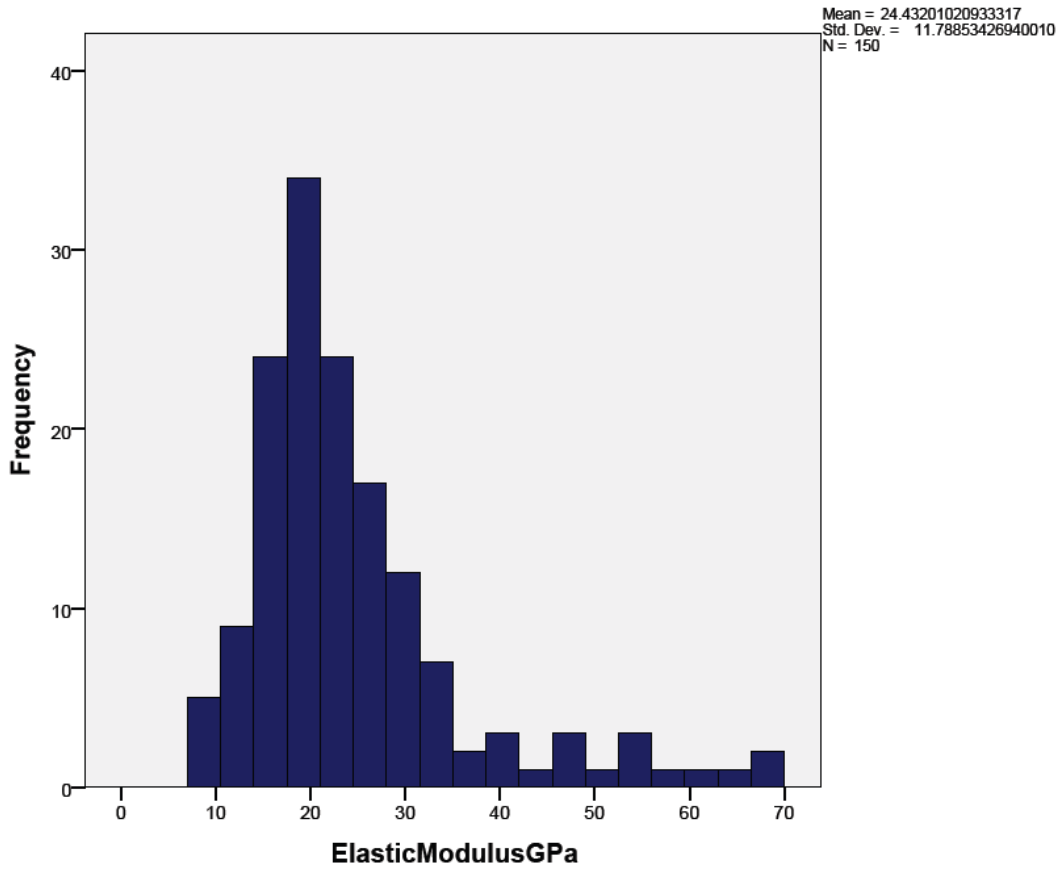


Figure 48: Frequency of elastic moduli of Portland cement with 50 mN max applied load

is the histogram of a nanoindentation test performed on hardened Portland cement paste with a maximum applied load of 50 mN. The average modulus of elasticity of this test is 24.4 GPa which is less than the test with the maximum applied load of 1.5 mN and the well-established modulus of Portland cement.

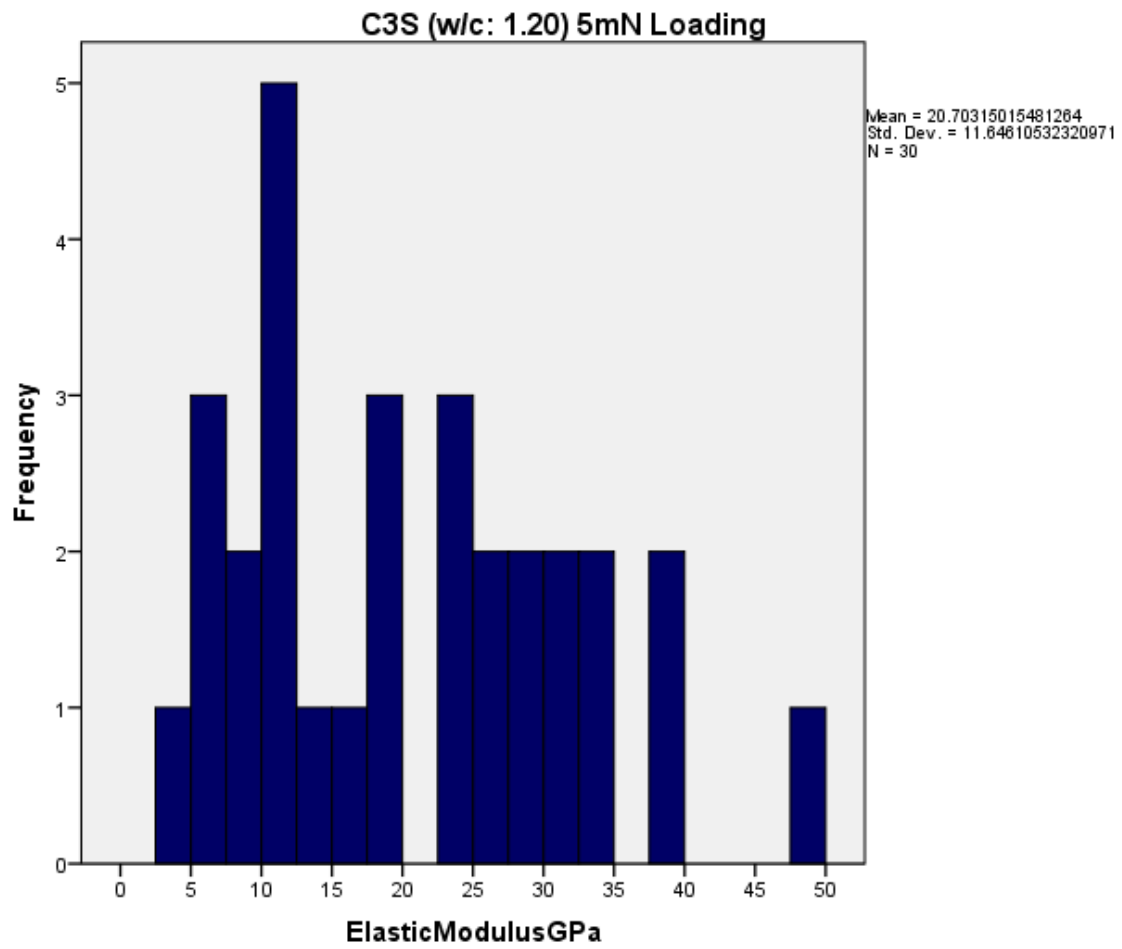


Figure 49: Frequency of elastic moduli of C₃S with 5 mN max applied load

3:1 C3S and Portland Cement 5mN Loading

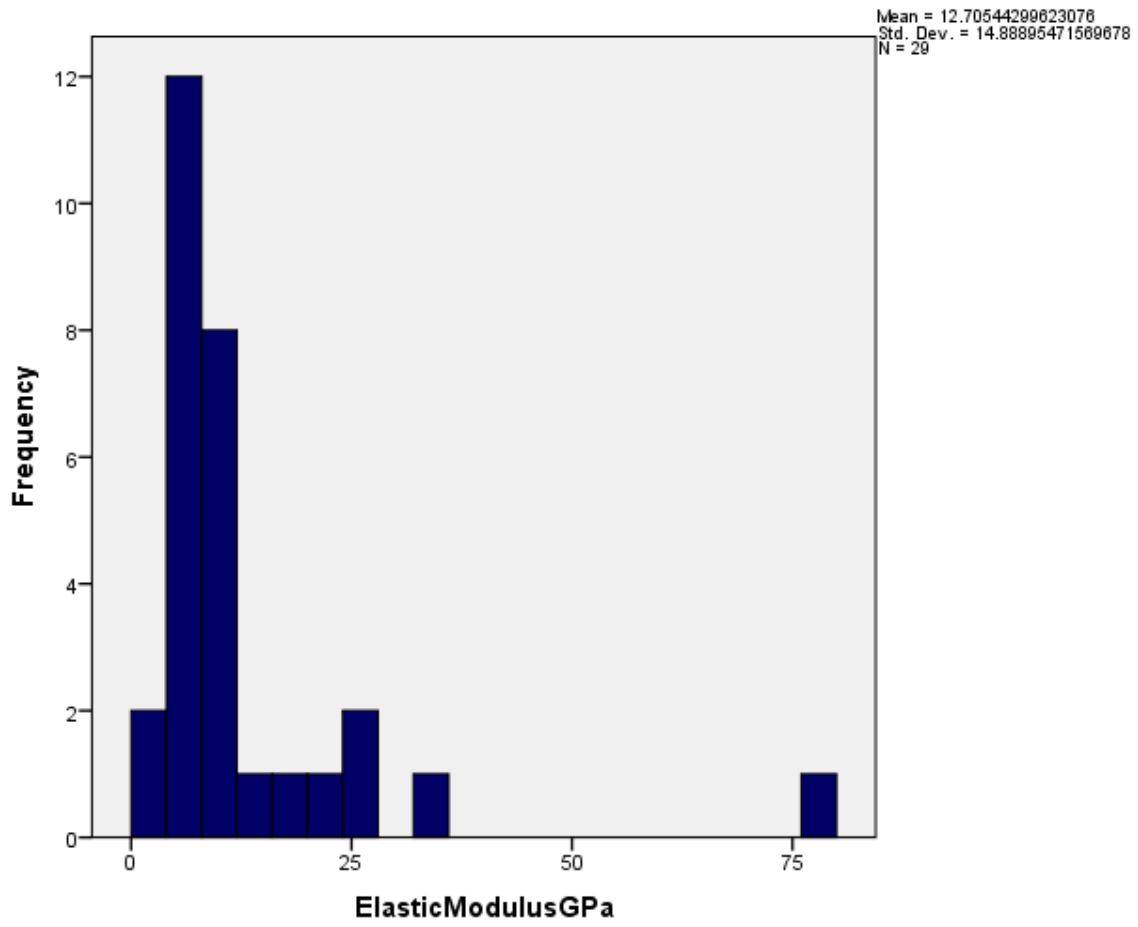


Figure 50: Frequency of elastic moduli of C_3S with 30% Portland cement with 5 mN max applied load

3:1 C3S and Portland Cement with Gypsum 5mN Loading

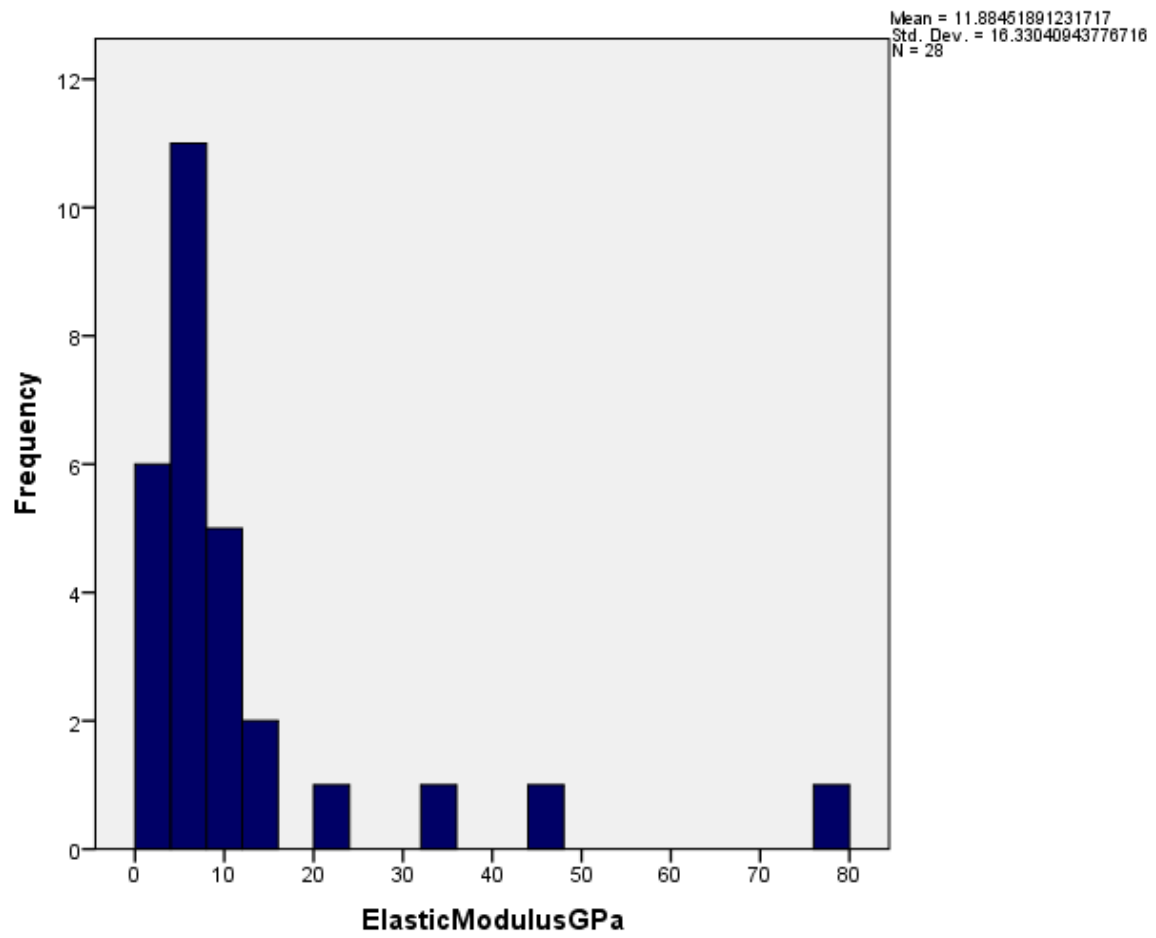


Figure 51: Frequency of elastic moduli of C₃S with 30% Portland cement and gypsum with 5 mN max applied load

C3S (w/c: 1.20, ERDC Polish) 5mN Loading

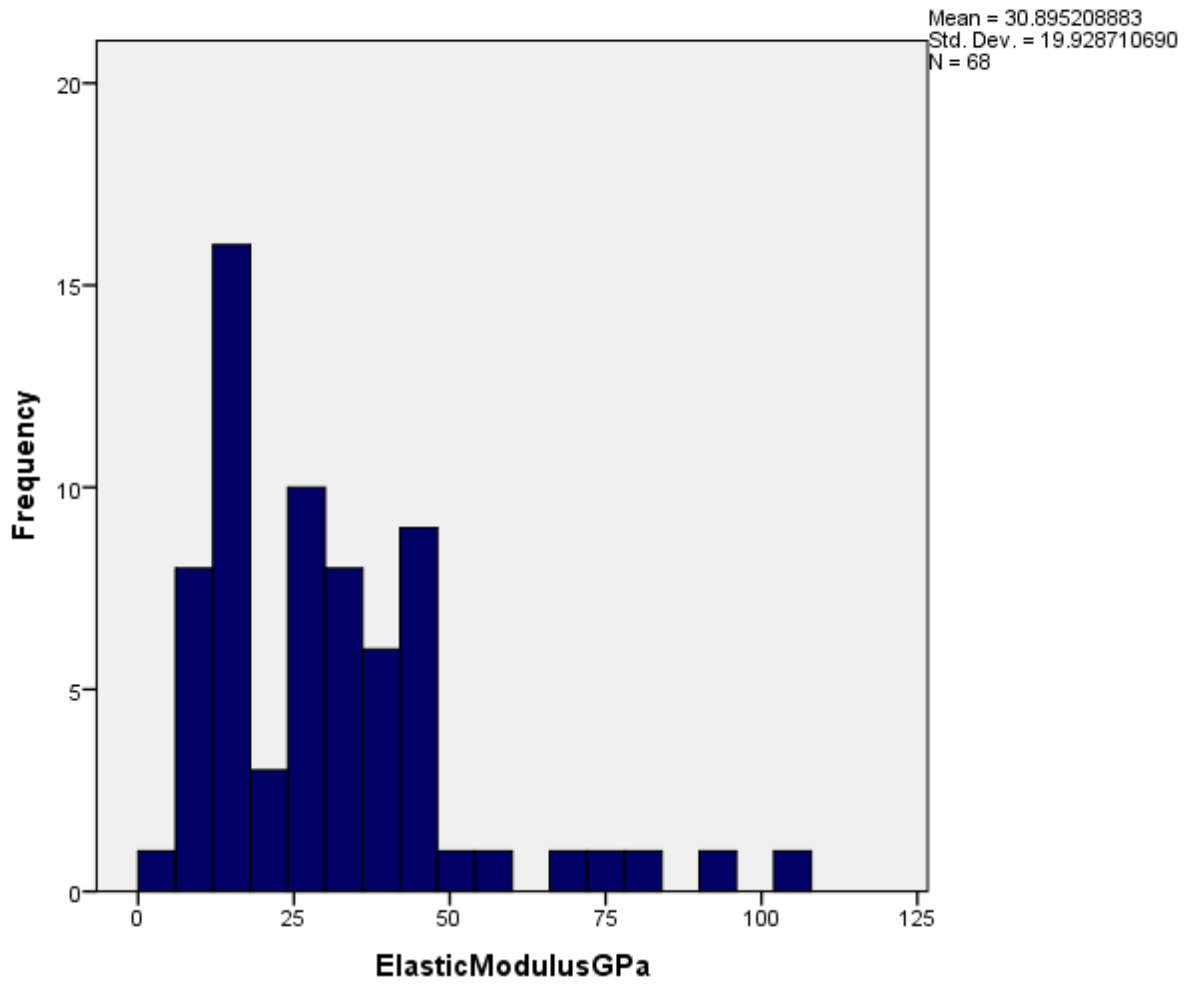


Figure 52: Frequency of elastic moduli of C₃S with 5 mN max applied load after ERDC preparation

4. CONCLUSION

Creating an accurate molecular model for Portland cement and its constituents has proven to be a difficult task, and there is still yet to be an exact, precise model. The large C-S-H model produced results that significantly varied among different combinations of forcefield and MD tool. However, with an elastic modulus of 33.27 GPa, applying the Dreiding forcefield using the GULP MD tool is the combination that most closely matches the experimental modulus (34.1 GPa). Modifying Hamid's Tobermorite 11Å model by changing the chain length proved to be beneficial in the study of deterioration of cement. This was accomplished by breaking the silicon chains and replacing the ends of the broken bonds with H atoms. As the Ca/Si ratio deviates farther from 1.00 (higher or lower), the structure becomes weaker (more damaged). AFM techniques were utilized in several methods to further understand the composition of hardened Portland cement paste. The two portions of C-S-H, LD C-S-H and HD C-S-H, were identified by taking a detailed look into the topographic images produced by the AFM. Phase contrast images from AFM were further analyzed with the creation of frequency distribution plots that were correlated to results obtained through XRD and MD simulations. The comparison between the phase contrast frequency distribution plots and the XRD results provided a rough correlation between the phase contrast angle and the components of

hardened Portland cement paste. This method was useful for determining where each of the cementitious constituents is located on the AFM images. The comparison between the phase contrast frequency distribution plot and the MD simulation results was based on the distribution of elastic moduli of the constituents of cement.

The main hydrating component and most abundant mineral in Portland cement is alite, so it is important to study the pure form of it, C_3S . Pure C_3S was created by heating a mixture of the chemicals of which C_3S is composed until a paste is formed, and then annealing the paste at a high temperature. The resulting substance was in a solid form that needed to be ground to a powder before XRD validation and hydration. The results from the XRD spectrum proved that C_3S had, in fact, been created.

Hydrating the newly created form of pure C_3S proved to be difficult due to the small particle sizes and high surface areas of the particles that require more water than common Type I/II Portland cement. The w/c ratio of 1.20 was decided upon for the analysis of the C_3S alone. However, other attempts were made to reduce the w/c ratio by adding Portland cement and gypsum to the powder with a w/c ratio of 1.00. The C_3S alone with the 1.20 w/c ratio provided nanoindentation results most closely related to Portland cement with an elastic modulus of 30.9 GPa, a value that proves this C_3S product is not stronger than Portland cement. This is believed to be due to presence of a high Ca/Si ratio which has proven to be detrimental to the mechanical performance of cement through MD simulations.

4.1. Future work

- Even though C_3S is presumably the most important component of Portland cement to study, there are still three others that can be manufactured and analyzed in a similar way to provide further insight into the study of nano cement. Following the same procedure for manufacturing C_3S described in Section 3.1, C_2S , C_3A , and C_4AF can be created for analysis through AFM and NI.
- The C_3S specimens prepared in this study are not perfect, and therefore, different techniques of manufacturing the C_3S powder and curing the C_3S paste should be attempted to reduce the w/c ratio.
- Steps will be taken towards developing “hand-shaking” algorithms for multi-scale modeling and characterization of cementitious materials. This can be accomplished using methods such as neural networking, the Cosserat theory of elasticity, and coarse graining techniques.

BIBLIOGRAPHY

- Accelrys, *Materials Studio Release Notes, Release 4.1*, Accelrys Software, Inc.: San Diego, 2006
- Al-Ostaz, A., et al. "A molecular dynamics and microporomechanics study on the mechanical properties of major constituents of hydrated cement." *Composites Part B: Engineering* 41.7 (2010): 543-549.
- Alkhateb, Hunain, Ahmed Al-Ostaz, and A. H. D. Cheng. "Geometric and simulation parameter effects on elastic moduli of multi-walled carbon nanotubes using molecular dynamics approach." *Proc. of the 23rd Technical Conf. of American Society for Composites*. 2008.
- Allen, Andrew J., Jeffrey J. Thomas, and Hamlin M. Jennings. "Composition and Density of Nanoscale Calcium–silicate–hydrate in Cement." *Nature Materials* 6 (2007): 311-16. Web.
- "American Mineralogist Crystal Structure Database." *American Mineralogist Crystal Structure Database*. N.p., n.d. Web. <<http://rruff.geo.arizona.edu/AMS/amcsd.php>>.
- Born, M., and Huang, K. (1954). *Dynamical theory of crystal lattices*, Oxford University Press, London.
- Constantinides, Georgios, F-J. Ulm, and K. Van Vliet. "On the use of nanoindentation for cementitious materials." *Materials and Structures* 36.3 (2003): 191-196
- Constantinides, Georgios, and Franz-Josef Ulm. "The effect of two types of CSH on the elasticity of cement-based materials: Results from nanoindentation and micromechanical modeling." *Cement and concrete research* 34.1 (2004): 67-80.

- De la Torre, Ángeles G., et al. "Crystal structure of low magnesium-content alite: Application to Rietveld quantitative phase analysis." *Cement and Concrete Research* 38.11 (2008): 1261-1269.
- Dormieux, Luc, and F. -J. Ulm. *Applied Micromechanics of Porous Materials*. Wien: Springer, 2005. Print.
- Gale, J. D., Rohl, A. L., "The General Utility Lattice Program (GULP)" *Molecular Simulation*, 29(5) pp.291-341 (2003).
- Hamid, S. A. "The crystal structure of the 11Å natural tobermorite Ca₂. 25 [Si₃O₇. 5 (OH) 1.5]· 1H₂O." *Zeitschrift für Kristallographie* 154.3-4 (1981): 189-198.
- Henderson, D. M., and H. S. Gutowsky. *A nuclear magnetic resonance determination of the hydrogen positions in Ca (OH) 2*. No. TR5. ILLINOIS UNIV URBANA NOYES CHEMICAL LAB, 1962.
- Huntzinger, Deborah N., and Thomas D. Eatmon. "A life-cycle assessment of Portland cement manufacturing: comparing the traditional process with alternative technologies." *Journal of Cleaner Production* 17.7 (2009): 668-675.
- Jennings, Hamlin M. "A model for the microstructure of calcium silicate hydrate in cement paste." *Cement and Concrete Research* 30.1 (2000): 101-116.
- Lin, Chiou-Kuo, Jong-Nan Chen, and Cheng-Chong Lin. "An NMR, XRD and EDS study of solidification/stabilization of chromium with Portland cement and C₃S." *Journal of hazardous materials* 56.1 (1997): 21-34.
- Mayo, S. L.; Olafson, B. D.; Goddard, W. A., III "DREIDING: A generic forcefield", *J. Phys. Chem.*, 94, 8897-8909 (1990).

- Němeček, Jiří (2012). Nanoindentation Based Analysis of Heterogeneous Structural Materials, Nanoindentation in Materials Science, Jiri Nemecek (Ed.), ISBN: 978-953-51-0802-3, InTech, DOI: 10.5772/50968.
- Neville, A. M. *Properties of Concrete*. 2nd ed. London: Pitman Limited, 1973. Print.
- Parker, S. C., de Leeuw, N. H., Bourova, E., and Cooke, D. J. (2001). "Application of lattice dynamics and molecular dynamics techniques to minerals and their surfaces." *Molecular modeling theory: Applications in the geosciences*, R. T. Cygan and J. D. Kubicki, eds., Geochemical Society/Mineralogical Society of America, 63–82.
- Rubenstein, Madeleine. "Mitigating Emissions from Cement." *TheGNCS.org*. Ed. Nico Tyabji. The Global Network for Climate Solutions, 2012. Web
- Selvam, R. Panneer, Vikramraja J. Subramani, Shanique Murray, and Kevin D. Hall. *Potential Application of Nanotechnology on Cement Based Materials*. Rep. no. MBTC DOT 2095/3004. N.p.: n.p., 2009.
- Song, C. R., Cho, H., Jung, Y.-H., Cheng, A. H. D., and Al-Ostaz, A. (2007). "Bridging molecular, particulate, and continuum mechanics for geomechanics application." *Proc., Geo-Denver 2007*, ASCE, Denver, 18–21.
- Sun, Huai. "COMPASS: An ab initio force-field optimized for condensed-phase applications overview with details on alkane and benzene compounds." *The Journal of Physical Chemistry B* 102.38 (1998): 7338-7364.
- Tchon, Johanna. "Bridging Nanoindentation And Macro Tensile Testing." *Nanovea.com*. N.p., 2010. Web.

- Tennis, Paul D., and Hamlin M. Jennings. "A model for two types of calcium silicate hydrate in the microstructure of Portland cement pastes." *Cement and Concrete Research* 30.6 (2000): 855-863.
- Wu, Weidong, et al. "Computation of elastic properties of Portland cement using molecular dynamics." *Journal of Nanomechanics and Micromechanics* 1.2 (2011): 84-90.
- Yao, Wu, et al. "Probing Nanostructure of Calcium Silicate Hydrate by AFM and Nanoindentation." *Key Engineering Materials* 539 (2013): 80-83.
- Zhu, Wenzhong, et al. "Nanoindentation mapping of mechanical properties of cement paste and natural rocks." *Materials characterization* 58.11 (2007): 1189-1198.

APPENDIX A

Molecular Structures/Molecular Dynamics Simulation Data

Table 6: Lattice parameters and information of MD structures

MD Structures				Lattice Parameters							Notes	Source
Type	Density	Atoms	Volume	Angle			Length					
				α	β	γ	A	B	C			
C ₃ S	3.09516	159	2166.20	104.982	94.6220	90.1070	11.6389	14.1716	13.6434	Alite	American Mineralogist	
CH	2.26937	5	54.2160	90.0000	90.0000	120.0000	3.58500	3.58500	4.87100	Portlandite	American Mineralogist	
C-S-H	2.43643	690	7517.69	92.6529	88.0105	123.367	13.1786	29.2308	23.3933		MIT	
Tobermorite 11Å	3.05073	98	939.208	90.0000	123.490	90.0000	7.39000	22.7790	6.69000	Ca/Si ratio: 1.25	Selvam et al	
Tobermorite 11Å	2.45733	74	939.208	90.0000	123.490	90.0000	7.39000	22.7790	6.69000	Ca/Si ratio: 0.83	Selvam et al	
Tobermorite 11Å	3.72339	112	939.208	90.0000	123.490	90.0000	7.39000	22.7790	6.69000	Ca/Si ratio: 1.0	Selvam et al	

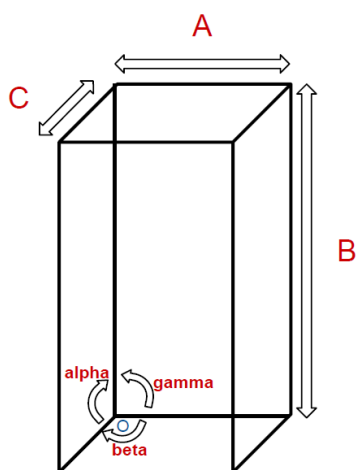


Figure 53: MD structures lattice parameter key

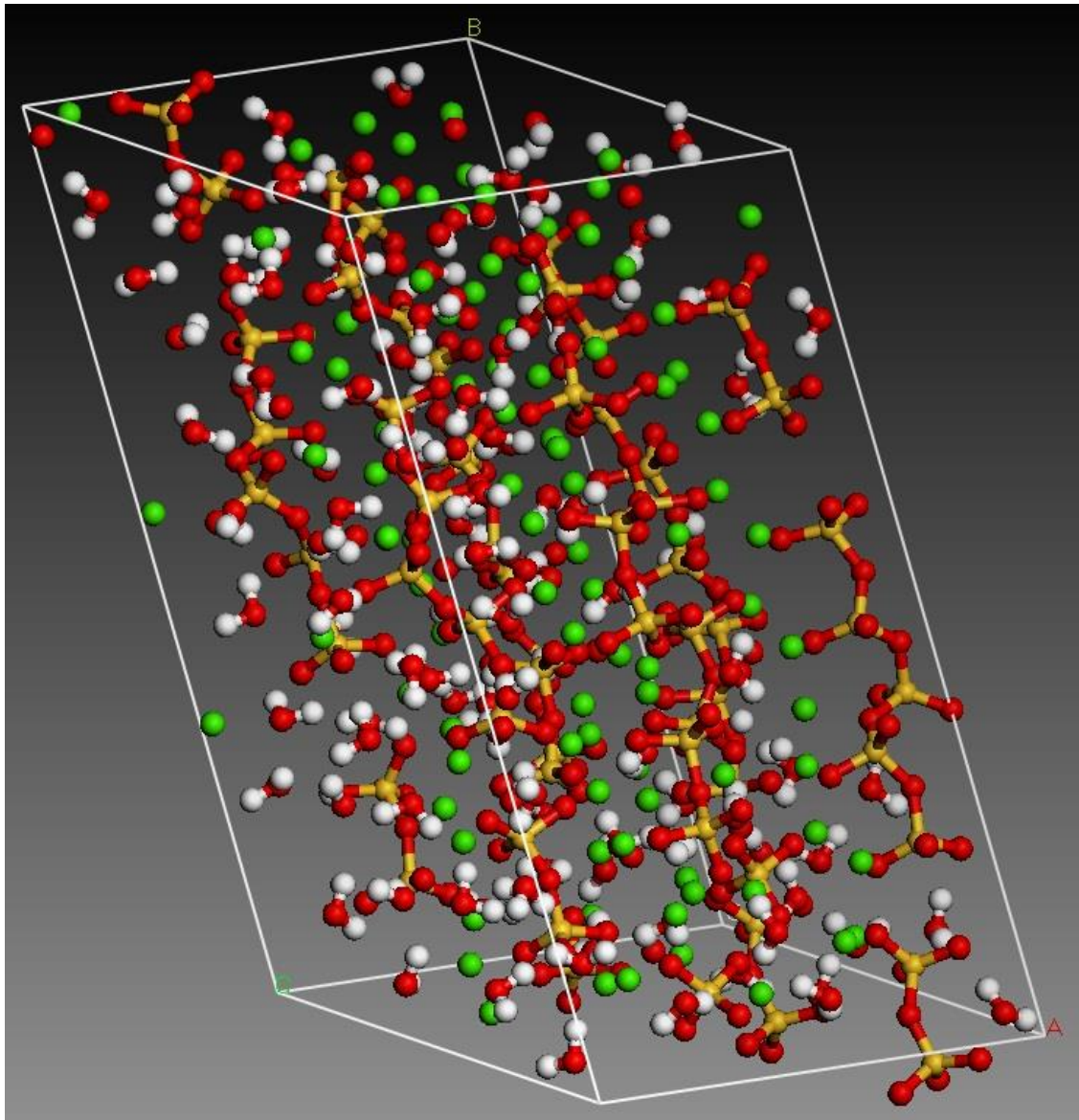


Figure 54: C-S-H unit cell from MIT

Table 7: C-S-H unit cell parameters

Type	C-S-H		
	Density	Atoms	Volume
	2.43643	690	7517.69
Angle	α	β	γ
	92.6529	88.0105	123.367
Length	A	B	C
	13.1786	29.2308	23.3933

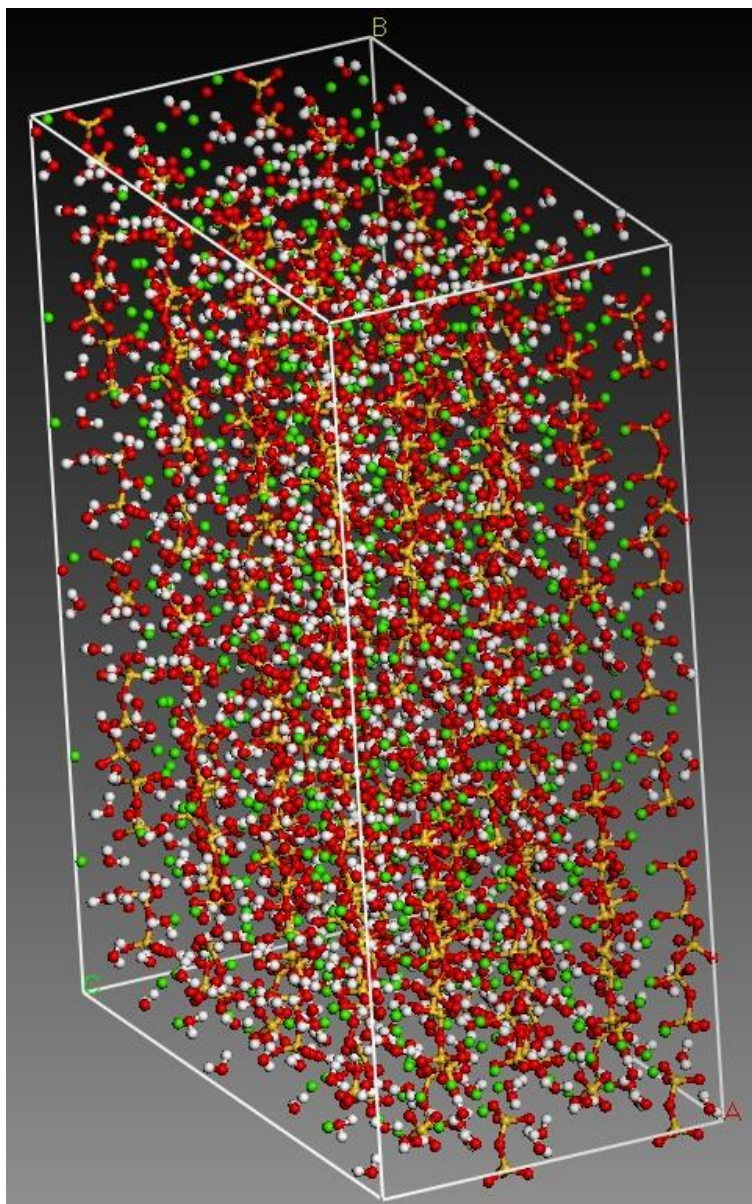


Figure 55: C-S-H Structure from MIT, 2x2x2 Supercell

Table 8: C-S-H supercell parameters

Type	C-S-H 2x2x2		
	Density	Atoms	Volume
	2.43643	5520	60141.6
Angle	α	β	γ
	92.6529	88.0105	123.367
Length	A	B	C
	26.3573	58.4616	46.7866

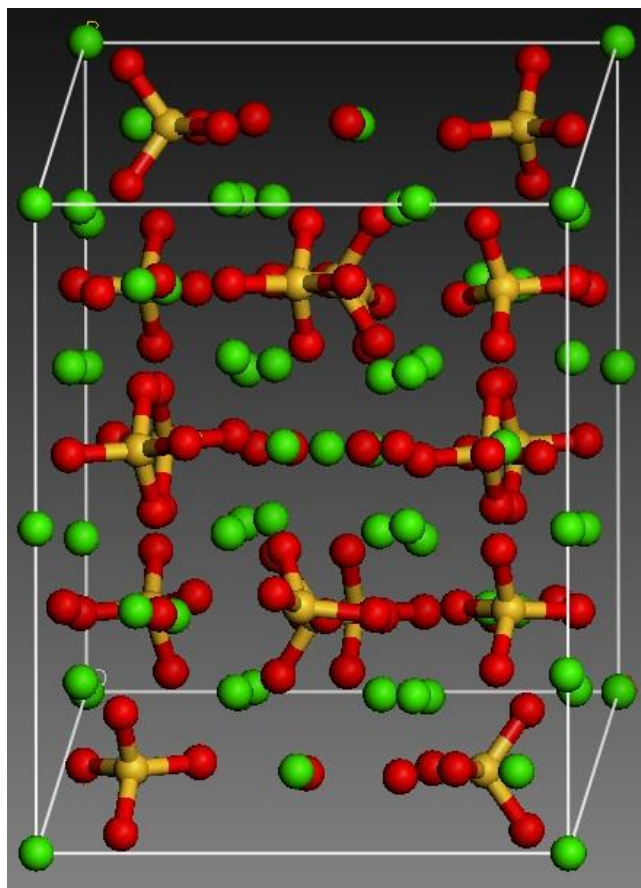


Figure 56: C₃S Unit Cell

The tricalcium silicate structure used in this research was obtained through the American Mineralogist Crystal Structure Database filed under the mineral name “Alite.” The structure was originally created by De la Torre et al. [2008], and the cell parameters are listed below.

Table 9: C₃S unit cell parameters

Type	C3S		
	Density	Atoms	Volume
	3.09516	159	2166.20
Angle	α	β	γ
	104.982	94.6220	90.1070
Length	A	B	C
	11.6389	14.1716	13.6434

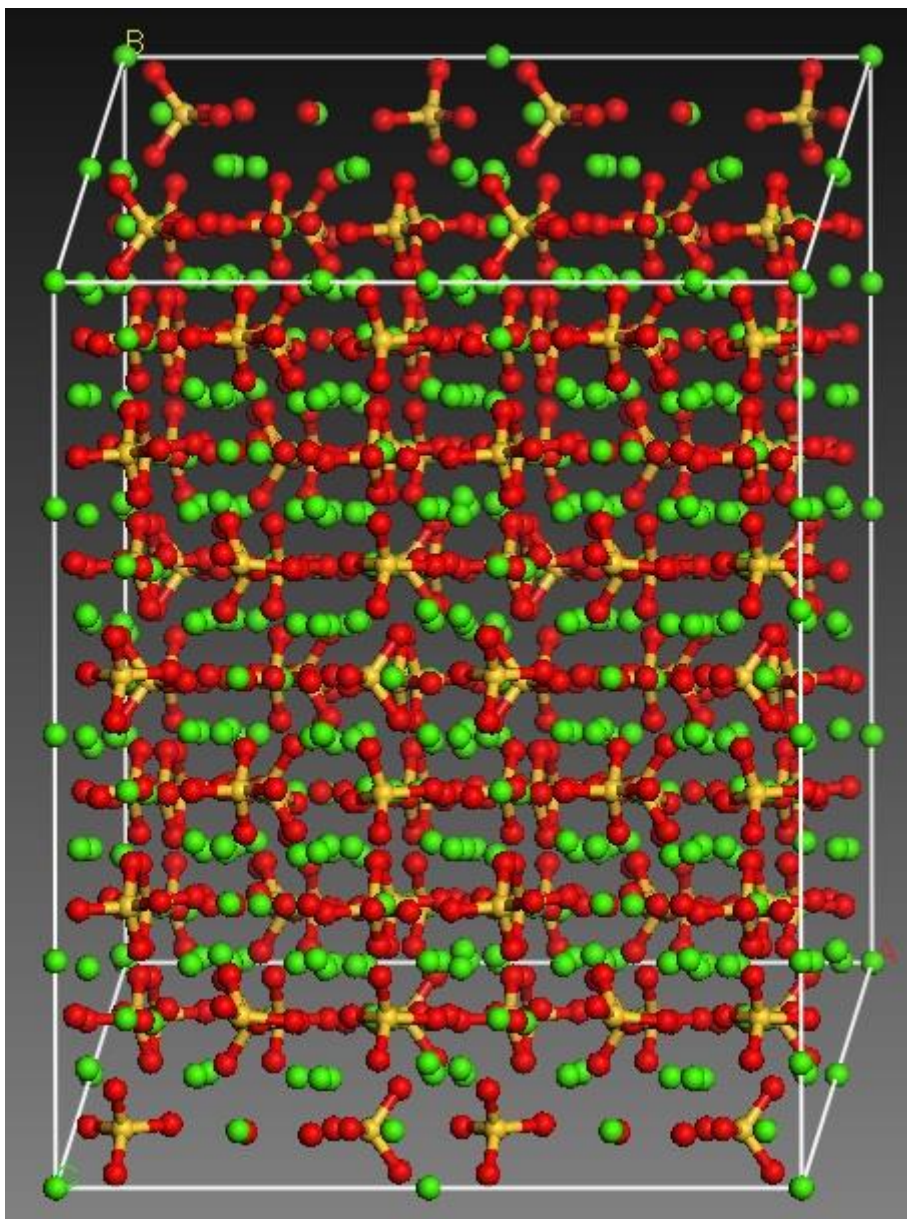


Figure 57: C_3S 2x2x2 Supercell

Table 10: C_3S supercell parameters

Type	C_3S 2x2x2		
	Density	Atoms	Volume
	3.09516	1272	17329.6
Angle	α	β	γ
	104.982	94.6220	90.1070
Length	A	B	C
	23.2778	28.3432	27.2868

VITA

University of Mississippi, University, MS

Bachelor of Science, Civil Engineering, May 2011